Eur. Phys. J. A (2017) **53**: 203
DOI 10.1140/epja/i2017-12402-7

THE EUROPEAN PHYSICAL JOURNAL A

Regular Article – Experimental Physics

Neutron capture measurements and resonance parameters of dysprosium

S.G. Shin[1], Y.U. Kye[1], W. Namkung[1], M.H. Cho[1], Y.-R. Kang[2,a], M.W. Lee[2], G.N. Kim[3,b], T.-I. Ro[4], Y. Danon[5], D. Williams[5], G. Leinweber[6], R.C. Block[6], D.P. Barry[6], and M.J. Rapp[6]

[1] Division of Advanced Nuclear Engineering, Pohang University of Science and Technology, Pohang, Gyeongbuk 37673, Republic of Korea
[2] Research Center, Dongnam Inst. of Radiological & Medical Sciences, Busan 46033, Republic of Korea
[3] Department of Physics, Kyungpook National University, Daegu 41566, Republic of Korea
[4] Dong-A University, Department of Physics, Busan 49315, Republic of Korea
[5] Department of Mechanical, Aerospace, and Nuclear Engineering, Rensselaer Polytechnic Institute, Troy, NY 12180-3590, USA
[6] Naval Nuclear Laboratory, Knolls Atomic Power Laboratory, P.O. Box 1072, Schenectady, NY 12301, USA

Received: 22 October 2016 / Revised: 27 September 2017
Published online: 19 October 2017 –
Communicated by A. Gade

Abstract. Neutron capture yields of dysprosium isotopes (^{161}Dy, ^{162}Dy, ^{163}Dy, and ^{164}Dy) were measured using the time-of-flight method with a 16 segment sodium iodide multiplicity detector. The measurements were made at the 25 m flight station at the Gaerttner LINAC Center at Rensselaer Polytechnic Institute. Resonance parameters were obtained using the multilevel R-matrix Bayesian code SAMMY. The neutron capture data for four enriched dysprosium isotopes and one natural dysprosium sample were sequentially fitted. New resonances not listed in ENDF/B-VII.1 were observed. There were 29 and 17 new resonances from ^{161}Dy and ^{163}Dy isotopes, respectively. Six resonances from ^{161}Dy isotope, two resonances from ^{163}Dy, and four resonances from ^{164}Dy were not observed. The capture resonance integrals of each isotope were calculated with the resulting resonance parameters and those of ENDF/B-VII.1 in the energy region from 0.5 eV to 20 MeV and were compared to the capture resonance integrals with the resonance parameters from ENDF/B-VII.1. A resonance integral value of the natural dysprosium calculated with present resonance parameters was 1405 ± 3.5 barn. The value is $\sim$ 0.3% higher than that obtained with the ENDF/B-VII.1 parameters. The distributions of the present and ENDF/B-VII.1 neutron widths were compared to a Porter-Thomas distribution. Neutron strength functions for ^{161}Dy and ^{163}Dy were calculated with the present resonance parameters and both values were in between the values of "Atlas of Neutron Resonances" and ENDF/B-VII.1. The present radiation width distributions of ^{161}Dy and ^{163}Dy were fitted with the χ^2 distribution by varying the degrees of freedom.

1 Introduction

Dysprosium is used in nuclear reactor systems because it has a very large thermal neutron absorption cross-section. Dysprosium alloyed with special stainless steels is attractive for control in nuclear reactors because of its ability to absorb neutrons readily without swelling or contracting over time and due to its high melting point [1]. Dysprosium is also one of the fission products from thermal fission of ^{235}U, ^{233}U, and ^{239}Pu. The fission products are accumulated in the reactor core by the burn-up of the nuclear fuel, and the poison effect is increased. Therefore, it is required to understand how dysprosium as both a poison and an absorbing material in the control rod has an effect on the neutron population in a nuclear reactor system over all energy regions.

Neutron capture yields of dysprosium isotopes were measured at the electron linear accelerator facility of the Rensselaer Polytechnic Institute (RPI) in the energy region from 10 to 1000 eV. The neutron capture data were combined with prior measurements of natural dysprosium in transmission at RPI [2]. The SAMMY multilevel R-matrix Bayesian code [3] was used to extract the resonance parameters.

The majority isotopes of ^{nat}Dy are ^{160}Dy, ^{161}Dy, ^{162}Dy, ^{163}Dy, and ^{164}Dy. Other authors observed resonance energies and/or spin assignments for resonances energies below 1000 eV for the isotopes, Liou *et al.* [4], Popov *et al.* [5], Beer *et al.* [6], and Kim *et al.* [7] for ^{160}Dy,

[a] e-mail: yeongrok@dirams.re.kr
[b] e-mail: gnkim@knu.ac.kr

Table 1. Isotopic composition of dysprosium samples.

Sample	Isotopic composition (%)						
	^{156}Dy	^{158}Dy	^{160}Dy	^{161}Dy	^{162}Dy	^{163}Dy	^{164}Dy
^{161}Dy	0.02	0.02	0.35	95.66	2.53	0.90	0.56
^{162}Dy	< 0.01	< 0.01	0.08	1.24	96.17	1.79	0.72
^{163}Dy	< 0.01	< 0.01	0.03	0.36	1.23	96.86	1.52
^{164}Dy	< 0.01	< 0.02	0.02	0.15	0.35	1.03	98.45
^{nat}Dy	0.06	0.10	2.34	18.9	25.5	24.9	28.2

Table 2. Characteristics of dysprosium samples. The atomic density was found from the mass and area.

Sample	Atomic Weight	Mass [mg]	Thickness [mm]	Area [mm^2]	Atoms/b
^{161}Dy	160.98 ± 0.10	536.1 ± 0.2	0.287 ± 0.003	315.4 ± 0.5	$6.36 \times 10^{-4} \pm 1.1 \times 10^{-6}$
^{162}Dy	161.91 ± 0.04	309.8 ± 0.2	0.295 ± 0.003	178.8 ± 0.4	$6.45 \times 10^{-4} \pm 1.5 \times 10^{-6}$
^{163}Dy	162.89 ± 0.08	555.7 ± 0.2	0.289 ± 0.004	315.9 ± 0.7	$6.50 \times 10^{-4} \pm 1.4 \times 10^{-5}$
^{164}Dy	163.87 ± 0.05	326.9 ± 0.2	0.310 ± 0.005	193.9 ± 2.2	$6.20 \times 10^{-4} \pm 6.9 \times 10^{-5}$
^{nat}Dy	162.49 ± 0.22	5026.9 ± 0.2	0.604 ± 0.011	1142.7 ± 0.8	$1.6304 \times 10^{-3} \pm 1.3 \times 10^{-6}$

Zimmerman *et al.* [8], Brunhart *et al.* [9,10], Mughabghab and Chrien [11], Karzhavina *et al.* [12,13], Liou *et al.* [4], Popov *et al.* [5], and Kim *et al.* [7] for ^{161}Dy, Zimmerman *et al.* [8], Mughabghab and Chrien [11], Liou *et al.* [4], and Kim *et al.* [7] for ^{162}Dy, Zimmerman *et al.* [8], Brunhart *et al.* [9,10], Brunner *et al.* [14], Mughabghab and Chrien [11], Slaughter *et al.* [15], Karzhavina *et al.* [12,13], Liou *et al.* [4], Popov *et al.* [5], and Kim *et al.* [7] for ^{163}Dy, and Zimmerman *et al.* [8], Sher *et al.* [16], Mughabghab and Chrien [11], and Liou [4] for ^{164}Dy. Recently, the resonance parameters for ^{164}Dy were obtained from capture and transmission experiments at RPI in the neutron energy region from 0.01 eV to 600 eV [2].

2 Experimental setup

The experiments were performed at the Gaerttner LINAC Center at RPI.

2.1 Detector and data acquisition

The experiments were performed under the same conditions as Kang's experiments [17] and only a short relevant description will be given here. During the experiment, the electron LINAC was operated at a repetition rate of 225 pps, a pulse width of 18 ns, and electron energy of $\sim$ 57 MeV. The Bare Bounce Target (BBT) [18] was used for this experiment. The BBT is made of tantalum plates and a 2.54 cm-thick polyethylene moderator and was developed to enhance the epithermal neutron production at RPI. A B_4C overlap filter with thickness of 0.021 atoms/barn was used to remove overlap neutrons from previous LINAC pulses.

The samples were placed at the center of the NaI(Tl) multiplicity detector located at a flight path distance of 25 m. The detector had a cylindrical shape with hole through the neutron path where the sample was placed in the center of the cylinder. The detector contains 20 liters of NaI(Tl) divided into 16 optically isolated segments. An annular liner composed of 99.4 wt% $^{10}B_4C$ ceramic surrounds the sample and absorbs neutrons which are scattered from the sample in the direction of the NaI(Tl) detector. The thickness of the liner is 1 cm. The efficiency to detect a neutron capture event of dysprosium samples for this detector was found to be in the range from 87%–97% [2]. The data acquisition system had a time bin width of 12.8 ns and a fixed dead time of 1.125 μs. Both the total energy deposited and observed cascade multiplicity were collected. In this experiment a total energy deposition greater than 1 MeV in all segments of the detector was considered a valid gamma capture event. Data were collected for each of the samples (including an empty sample holder) in multiple files containing data for about 10 minutes of accelerator run time. A total beam time of 54 hours was used for this experiment.

2.2 Samples

The isotopic compositions and characteristics of the four isotopically-enriched dysprosium metallic samples used in the experiments are listed in tables 1 and 2. The isotopic abundances of the elemental sample were taken from ref. [19].

Transmission data from the 0.0254 cm (10 mil) thick natural dysprosium sample were used to get the normalization factor and conduct combined fitting with the capture data. The precise description about the sample is in ref. [2].

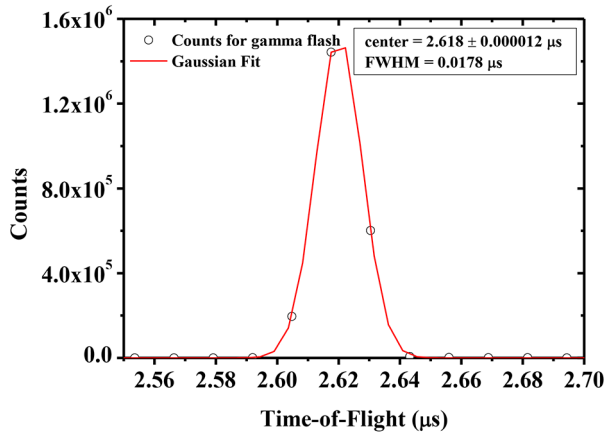

Fig. 1. Gaussian fit of the gamma flash data. The center corresponds to t_0 plus the flight time of the gammas, and FWHM corresponds to the electron burst width of the LINAC.

3 Data reduction

The yield data reduction was performed with RPI's Cross-Section Data Reduction (RPIXDR) computer code which is an internal code at RPI. The RPIXDR program produces dead time-corrected, monitor-normalized, run-summed, and grouped data files [20]. The data were corrected for a dead time of 1.125 μs, set by the system electronics. The max dead time correction was 0.5%, and the probability for pulse pileup was negligible even in resonance peaks where the count rate is high. The basic TOF channel width was 0.0128 μs and the TOF data for the capture yield was grouped by RPIXDR. The channel width increased at each of the following energies 1000 eV, 500 eV, and 100 eV to 0.0256 μs, 0.0512 μs, and 0.1024 μs, respectively.

3.1 Neutron energy

In this experiment the neutron energy was assumed to be non-relativistic. The non-relativistic energy given by eq. (1) is appropriate for incident neutron energies below 1 keV,

$$E_i = \left(\frac{72.296L}{t_i - t_0}\right)^2, \qquad (1)$$

where E_i = neutron energy in TOF channel i in eV, L = flight-path in m, t_i = arrival time of the neutron in μs, t_0 = time when the electron pulse impinges on the target in μs.

The flight path distance L was 25.5686 m and t_0 was determined from a separate measurement of the gamma flash. The gamma flash is the burst of γ flash generated along with the neutrons in the Ta target. The γ flash data and the Gaussian fitted curve are shown in fig. 1. The value of t_0 was 2.545 μs after correcting for the flight time of the gammas from the source to the detector.

The Full Width at Half Maximum (FWHM) of the Gaussian fit to the electron burst width of LINAC was found to be 17.8 ns, which was used as the burst width during the resonance parameter fitting process.

3.2 Capture yield

The data were reduced in the same manner as in Kang *et al.* [17]. The capture yield, Y_i, in TOF channel i can be expressed by

$$Y_i = \frac{C_i - B_{sm,i}}{K\phi_{sm,i}}, \qquad (2)$$

where C_i = counting rate with the sample, $B_{sm,i}$ = smoothed, counting rate without sample (background), K = neutron flux normalization and detection efficiency normalization, $\phi_{sm,i}$ = smoothed, background-subtracted neutron flux shape.

The counting rate for background was measured using an empty sample holder. As mentioned in sect. 2, scattered neutrons from the sample were absorbed by the boron carbide liner, and the frame-overlap background was removed by the B_4C filter. Dy capture data were discriminated such that the total deposited gamma energy exceeded 1 MeV, removing the 478 keV γ-rays from the $^{10}B(n,\alpha_1)$ reaction in the liner.

To determine the incident neutron flux shape, a 97.4 wt% enriched $^{10}B_4C$ sample, 2.54 mm thick, was placed at the sample position inside the capture detector and the 478 keV γ-rays from $^{10}B(n,\alpha_1)$ reactions were recorded during the measurement. In the energy range of interest the $^{10}B(n,\gamma)$ reaction cross section is several orders of magnitude ($\sim$ 4) smaller than the $^{10}B(n,\alpha_1)$ reaction, and thus gammas from capture reaction in the sample used for flux measurement or from the B_4C liner are negligible. The counting rate from the empty sample holder run was also subtracted from that of the $^{10}B_4C$ measurement. The $^{10}B_4C$ sample absorbed all the incident neutrons at low energies, but some neutrons passed through the $^{10}B_4C$ sample without neutron capture at high energy. Therefore, a correction factor accounting for the fraction of neutrons that were not captured in the $^{10}B_4C$ sample was applied to accurately portray the incident neutron flux. A flux normalization factor was required because the magnitude of the incident neutron flux could not be quantified using the $^{10}B_4C$ sample. The calculation of the flux normalization factor is described in detail in sect. 3.3. The background and flux were smoothed by averaging the adjacent points to reduce the statistical fluctuations. There were no surrounding materials with the resonance structure to change the neutron flux shape. Therefore, the flux shape was not distorted by the smoothing. The measured capture yield and its uncertainties were used as input parameters for the SAMMY data analysis code. Capture data were not used below 10 eV due to excessive background.

3.3 Normalization and detector efficiency

The magnitude of neutron flux for the capture data was normalized directly with a saturated capture resonance

Table 3. The normalization factors and relative detector efficiencies relative to the ^{161}Dy yield data.

Sample	Resonance energy [eV]	Normalization factor	Normalization factor error	Relative detector efficiency [%]	Detector efficiency error [%]
Natural	18.50	0.668	0.014		
^{161}Dy	18.50	0.724	0.01	100	2
^{162}Dy	5.45	1.158	0.015	86	2
^{163}Dy	59.06	0.774	0.012	92	2
^{164}Dy	147.13	1.162	0.028	88	2

for ^{162}Dy at the 5.4 eV resonance; the Γ_γ was 147.4 meV, and the Γ_n was 21.2 meV. Other isotopes could not be directly normalized because they had no saturated resonances; for these isotopes the capture data were normalized with the resonance parameters from the SAMMY fit to the 10 mil natural dysprosium (8.05×10^{-4} atoms per barn) transmission data at energies of 18.5 eV for ^{161}Dy, and 59.06 eV for ^{162}Dy. In case of ^{164}Dy, resonance parameters at 147.14 eV obtained by Block *et al.* [2] from transmission and capture data were used to obtain the normalization factor; the details about the measurements and data reduction of transmission of the 10 mil natural Dy sample are available in Block *et al.* [2].

The detector efficiency varies with each isotope depending on the neutron binding energy and gamma multiplicity and cascade spectrum. The $^{\text{nat}}$Dy capture yield data were normalized to the transmission of the 10 mil $^{\text{nat}}$Dy sample using the 18.5 eV resonance in ^{161}Dy. The same resonances used for the normalizations of the isotopes and natural capture yield data were used to find the detector efficiency for each isotope. The detector efficiency was fit to the normalized $^{\text{nat}}$Dy experimental data with the resonances using the SAMMY. The detector efficiency that resulted in the best fit was used in the SAMMY analysis. In this analysis, we assumed no efficiency variations from resonance to resonance in the same isotope because all multiplicities were summed. Since the total gamma cascade energy does not vary with the spin, the efficiency does not depend on the resonance spin.

The results of this procedure are documented in table 3. The errors on the normalization factors and detector efficiencies in table 3 came from the SAMMY fit. The relation between the detector efficiencies and the binding energy was observed to be linear within ±5%.

4 Data analysis

4.1 Resolution function

Resolution broadening is an experimental effect and reflects the distribution in the neutron flight path-length, electron burst width, time-of-flight channel width, and all other experimental conditions. Since SAMMY is a shape fitting analysis code, it is important to know the resolution function, which changes the resonance shape. This resonance parameter analysis was performed using the resolution functions determined by Barry [21] for the same neutron producing target (epithermal BBT) and similar experimental conditions. In ref. [21] a ^{238}U sample was used as the benchmark material. Therefore, a natural metallic uranium capture experiment was performed to confirm whether the parameters were correct. The ^{238}U sample data also were used to verify the flight path length L and t_0. Resonance shapes and energies determined by the assumption that the neutron energy is non-relativistic, resulted in good agreement between the measured data and ^{238}U resonance parameters from ENDF/B-VII.1 [22], as shown in fig. 2. This procedure serves as validation of the TOF energy calibration (L and t_0) and the SAMMY resolution function.

4.2 SAMMY analysis

The fitting procedure was the same technique implemented by Barry [21]. All resonance energies and neutron widths were varied by sequentially fitting the transmission and capture yield data, with the covariance matrix file, which was generated by the previous iteration. If a resonance included a significant quantity of scattering the resonance was regarded as sensitive to the radiation width and was fitted. The method to determine which radiation widths to vary was based on a sensitive factor defined as follows [21]:

$$S_\gamma = \frac{\Gamma_\gamma}{\Gamma_n}\,. \tag{3}$$

Γ_γ and Γ_n were taken from ENDF-B/VII.1 [22]. When $S_\gamma < 5$, the resonance was regarded sensitive to Γ_γ and both Γ_γ and Γ_n were solved simultaneously. When $S_\gamma \geq 5$, the resonance was considered insensitive to Γ_γ and only Γ_n was solved.

A combined fit was performed on the transmission, natural sample, and dysprosium isotopes data. Each data set was fitted sequentially with the covariance matrix file from the previous samples in the sequence. The resonance parameters of ^{160}Dy were varied together because it is contained by 2.34% of the natural sample. However, the resonance parameters of ^{156}Dy and ^{158}Dy listed in the parameter file of SAMMY were fixed to ENDF/B-VII.1 values during the fitting because of their low abundances (0.06% and 0.1% for natural dysprosium).

Before the final fit iteration, the average radiation width $\langle\Gamma_\gamma\rangle$ and uncertainty $\langle\Delta\Gamma_\gamma\rangle$ for each dysprosium isotope were calculated by using a weighted average technique using only the sensitive radiation widths. The radiation widths of new resonances were set to the average

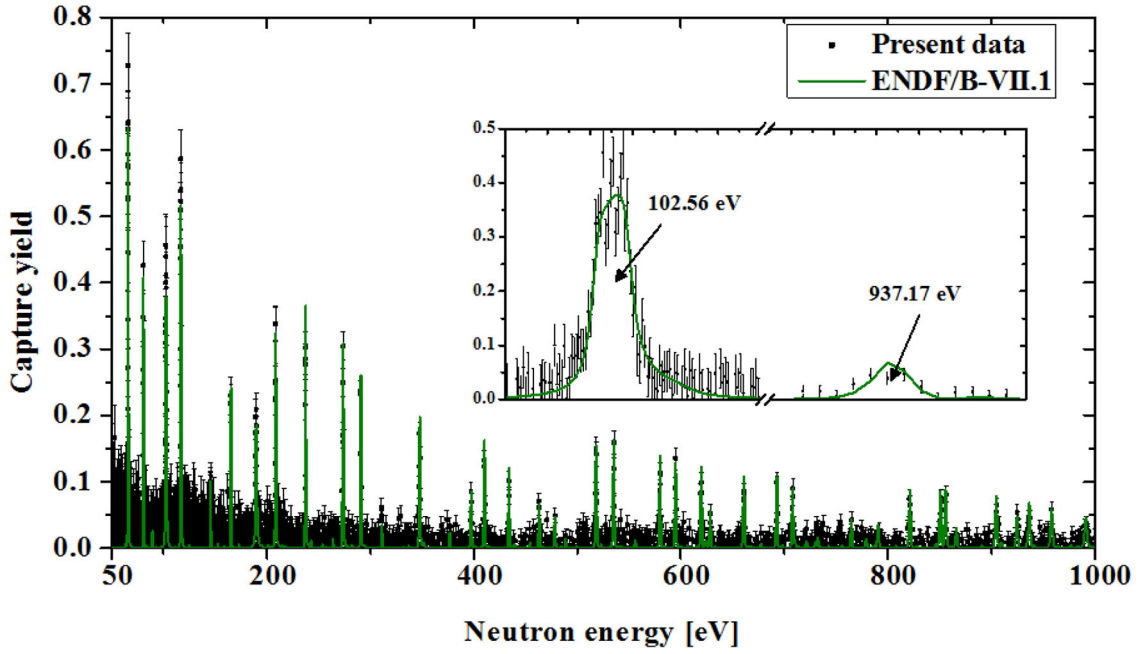

Fig. 2. Capture yield data of ^{238}U and the SAMMY plot using ENDF/B-VII.1 resonance parameters of ^{238}U and Barry's resolution function [21].

Table 4. Average radiation width $\langle \Gamma_\gamma \rangle$ for each dysprosium isotope in the energy range from 10 to 1000 eV. All data included were from resonances sensitive to the value of the radiation width based on the criterion $S_\gamma < 5$, where S_γ is defined in eq. (3).

Dysprosium isotope	Average radiation width $\langle \Gamma_\gamma \rangle \pm \Delta\langle \Gamma_\gamma \rangle$ [meV]	The number of sensitive radiation widths
^{161}Dy	112 ± 1	100
^{162}Dy	90 ± 2	13
^{163}Dy	108 ± 2	70
^{164}Dy	85 ± 4	5

values presented in table 4. The radiation widths of insensitive resonances were kept at the ENDF/B-VII value.

If a new resonance not listed on ENDF/B-VII.1 was observed, the average radiation width was assigned as the radiation width of that resonance and only the resonance energy and neutron width were allowed to be varied. After the final parameters from the SAMMY analysis were determined, it was confirmed how these parameters fit each sample individually. This was accomplished by calculating a theoretical curve for each sample with the final parameters using the "Do not solve Bayes equation" command in SAMMY. The chi-squared values were generated by this process, and results are presented in the next section.

5 Results

5.1 Resonance parameters

The neutron width, Γ_n, radiation width, Γ_γ, and resonance energy, E_0, were extracted from the capture yields of four enriched dysprosium isotopes, the 20 mil natural sample, and the transmission data from the 10 mil natural sample. Figure 3 shows capture yield from the 20 mil natural dysprosium sample, capture yield from the four enriched isotopic samples, and transmission from the 10 mil natural Dy sample with the fitted curves obtained from the SAMMY program. A 0.041 in thick (0.104 cm) Mn-Cu alloy (80% Mn-20% Cu) sample was used for the determination of the time-dependent background during the transmission experiment [2]. Therefore, the neutron flux intensity goes to zero near the Mn strong resonance at 330 eV. The transmission data in this region were not used in the SAMMY analysis. In this region, the combined fit was performed only with natural and isotope yield data.

The final resonance parameters deduced from the previously described analysis in the energy range between 10 eV and 1000 eV are listed in tables 5–9. The resonance parameters of ENDF/B-VII.1 [22] are also listed on tables 5–9 to compare with the final resonance parameters. The uncertainties of the resonance parameters in tables 5–9 are purely statistical errors taken directly from the SAMMY fit. The sixth column in tables 5–9 indicates the source of Γ_γ, *i.e.*, fitted from the data (FIT), fixed to an average value (AVG), or fixed to the value of

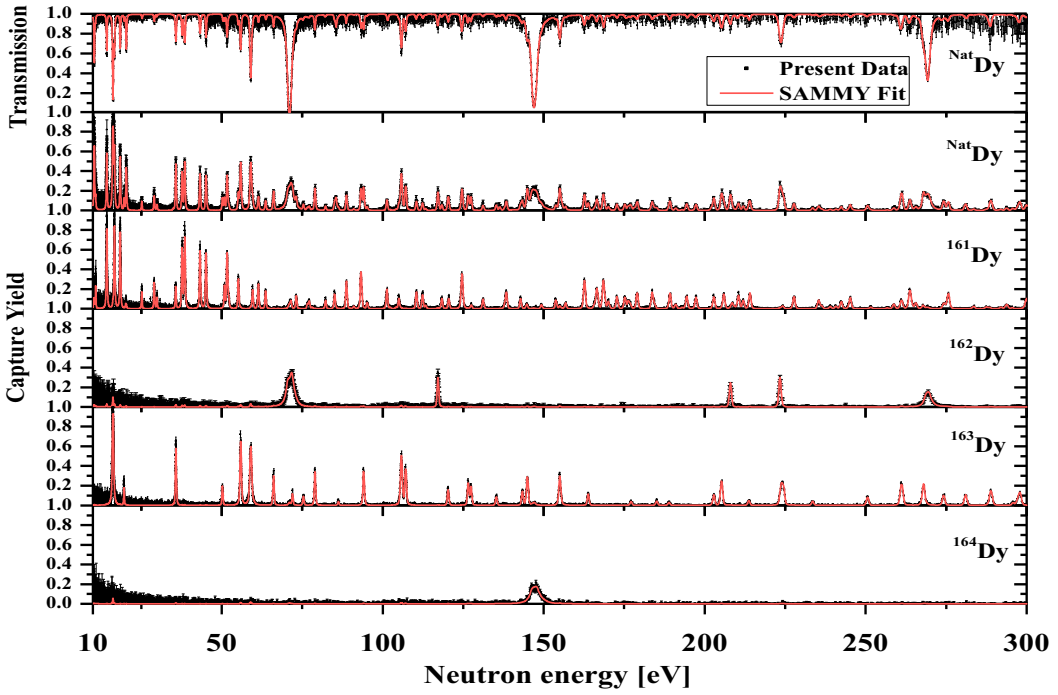

(a)

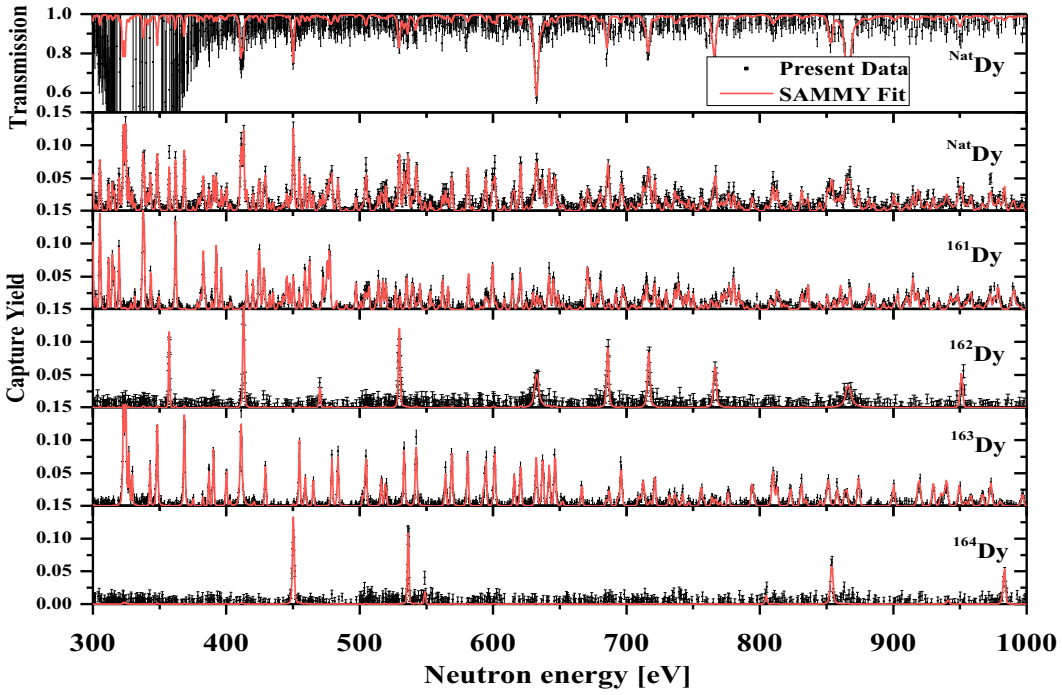

(b)

Fig. 3. Transmission data of the natural sample and capture yield data of natural and isotopic data (black points) in the neutron energy region (a) from 10 to 300 eV and (b) from 300 to 1000 eV. The red curves were plotted using the final resonance parameters.

Table 5. Resonance parameters for ^{160}Dy isotopes compared with ENDF/B-VII.1.

E_0 [eV]			Γ_γ [meV]				Γ_n [meV]			J value	
$E_{0,\mathrm{RPI}}$	$\Delta E_{0,\mathrm{RPI}}$	$E_{0,\mathrm{ENDF}}$	$\Gamma_{\gamma,\mathrm{RPI}}$	$\Delta\Gamma_{\gamma,\mathrm{RPI}}$	Γ_γ source	$\Gamma_{\gamma,\mathrm{ENDF}}$	$\Gamma_{n,\mathrm{RPI}}$	$\Delta\Gamma_{n,\mathrm{RPI}}$	$\Gamma_{n,\mathrm{ENDF}}$	RPI	ENDF
10.5	0.02	10.5	100.0		ENDF	100.0	25.4	0.5	16.5	0.5	0.5
20.4	0.03	20.5	71.2	5.5	FIT	105.8	37.5	1.0	31.0	0.5	0.5
34.9	0.1	34.9	105.8		ENDF	105.8	1.2	0.1	1.2	0.5	0.5
73.2	0.1	73.1	105.8		ENDF	105.8	7.0	0.7	6.5	0.5	0.5
85.6	0.0	85.6	98.6	8.9	FIT	112.0	93.8	6.8	91.0	0.5	0.5
115.6	0.2	115.6	105.8		ENDF	105.8	2.0	0.2	2.0	0.5	0.5
136.5	0.0	136.4	95.9	9.5	FIT	96.0	26.6	2.3	26.0	0.5	0.5
155.7	0.0	155.7	103.5	10.2	FIT	105.0	79.2	7.1	85.0	0.5	0.5
178.3	0.1	178.3	120.1	12.0	FIT	120.0	30.0	2.7	30.7	0.5	0.5
202.2	0.1	202.2	105.6	10.5	FIT	106.0	31.8	3.1	31.3	0.5	0.5
246.3	0.2	246.3	105.8		ENDF	105.8	8.8	0.9	8.8	0.5	0.5
272.0	0.3	271.9	105.8		ENDF	105.8	4.4	0.4	4.3	0.5	0.5
320.8	0.3	320.7	105.8		ENDF	105.8	13.0	1.3	13.1	0.5	0.5
341.2	0.1	341.2	105.9	9.9	FIT	105.8	391.3	37.9	390.0	0.5	0.5
379.5	0.1	379.3	104.1	9.7	FIT	105.8	291.9	29.0	292.0	0.5	0.5
394.4	0.2	394.3	105.8	10.6	FIT	105.8	60.0	5.9	60.0	0.5	0.5
398.7	0.1	398.8	103.0	9.8	FIT	105.8	205.9	20.0	210.0	0.5	0.5
429.7	0.2	430.1	109.1	10.8	FIT	110.0	112.4	11.1	114.0	0.5	0.5
522.6	0.2	522.2	105.6	10.4	FIT	107.0	133.4	13.1	133.0	0.5	0.5
577.2	0.4	577.4	100.1	10.0	FIT	100.0	36.1	3.6	3.6	0.5	0.5
591.0	0.5	590.0	105.8		ENDF	105.8	8.5	0.9	0.9	0.5	0.5
625.8	0.5	625.6	105.8		ENDF	105.8	8.0	0.8	0.8	0.5	0.5
653.5	0.5	653.6	105.8		ENDF	105.8	5.6	0.6	0.6	0.5	0.5
679.4	0.4	679.5	107.1	10.6	FIT	105.8	733.4	73.3	71.3	0.5	0.5
704.0	0.3	703.6	109.2	10.9	FIT	105.8	912.2	92.0	97.1	0.5	0.5
729.4	0.4	729.6	120.5	12.1	FIT	120.0	113.6	11.3	11.5	0.5	0.5
737.2	0.6	736.4	108.5	10.8	FIT	105.8	1269.1	126.9	127.3	0.5	0.5
817.6	0.6	817.2	105.8	10.6	FIT	105.8	32.1	3.2	3.2	0.5	0.5
844.9	0.6	845.2	106.2	10.6	FIT	105.8	110.5	11.1	11.1	0.5	0.5
868.9	0.7	868.6	107.0	10.7	FIT	105.8	157.4	15.7	15.8	0.5	0.5
889.1	0.7	889.1	105.8		ENDF	105.8	17.9	1.8	1.8	0.5	0.5
972.2	0.7	972.0	105.8		ENDF	105.8	6.9	0.7	0.7	0.5	0.5
988.7	0.7	989.3	106.2	10.6	FIT	105.8	88.6	8.9	8.8	0.5	0.5

ENDF/B-VII.1 (ENDF). The column labeled "J value" is the total angular momentum of the compound taken from ENDF/V-VII.1 and used for the SAMMY analysis. However, for the newly observed resonances, the spin value that resulted in the best fit to the experimental data was chosen.

Above 600 eV the boron carbide liner in the multiplicity detector is no longer black, and neutrons can enter the NaI and be captured. The contributions of the scattered neutron were estimated with a lead sample and MCNP Polimi [23]. The MCNP Polimi was used for the additional estimation of the slowing down of the scattered neutron in the sample. The false capture curve from the scattered neutron is shown in ref. [24]. The efficiency to record a scattering event as capture is less than 2% below 600 eV and less than 3% between 600 eV to 1000 eV.

All the measured resonances in this region were assigned as s-wave resonances in the ENDF/B-VII.1 evaluation. Therefore, new resonances were also regarded as s-wave resonances. We observed 29 and 17 new resonances not listed in ENDF/B-VII.1 from ^{161}Dy and ^{163}Dy isotopes, respectively. Six resonances from the ^{161}Dy isotope (12.65, 48.8, 485.31, 574.65, 587.17, and 803.87 eV), two resonances from ^{163}Dy (307.1 and 660.4 eV), and four resonances from ^{164}Dy (227.57, 479.39, 740.91, and 925.9 eV) listed in ENDF/B-VII.1 were not observed.

Table 6. Resonance Parameters for ^{161}Dy Isotopes Compared with ENDF/B-VII.1.

E_0 [eV]			Γ_γ [meV]				Γ_n [meV]			J value	
$E_{0,\mathrm{RPI}}$	$\Delta E_{0,\mathrm{RPI}}$	$E_{0,\mathrm{ENDF}}$	$\Gamma_{\gamma,\mathrm{RPI}}$	$\Delta\Gamma_{\gamma,\mathrm{RPI}}$	Γ_γ source	$\Gamma_{\gamma,\mathrm{ENDF}}$	$\Gamma_{n,\mathrm{RPI}}$	$\Delta\Gamma_{n,\mathrm{RPI}}$	$\Gamma_{n,\mathrm{ENDF}}$	RPI	ENDF
10.3	0.01	10.3	106.8		ENDF	106.8	0.2	0.02	0.3	2	2
10.9	0.004	10.9	106.8		ENDF	106.8	0.5	0.02	0.4	3	3
unobserved		12.7	unobserved			106.8	unobserved		00.05	unobserved	3
14.3	0.002	14.3	124.0		ENDF	124.0	7.9	0.1	7.4	2	2
16.7	0.001	16.7	116.0		ENDF	116.0	7.4	0.1	6.3	3	3
18.5	0.002	18.5	114.0		ENDF	114.0	10.0	0.1	10.2	2	2
20.2	0.03	20.2	106.8		ENDF	106.8	0.3	0.0	0.4	2	2
25.2	0.01	25.2	102.0		ENDF	102.0	1.5	0.1	1.4	2	2
29.1	0.004	29.0	126.0		ENDF	126.0	3.4	0.1	3.2	2	2
29.9	0.01	29.9	116.0		ENDF	116.0	0.9	0.0	0.8	3	3
35.7	0.01	35.7	106.8		ENDF	106.8	2.4	0.1	2.4	3	3
37.7	0.002	37.7	118.0		ENDF	118.0	11.6	0.2	9.6	3	3
38.5	0.002	38.5	110.0		ENDF	110.0	17.1	0.2	12.3	3	3
43.3	0.002	43.3	117.0		ENDF	117.0	13.5	0.2	11.1	3	3
45.2	0.003	45.1	108.0		ENDF	108.0	20.7	0.3	14.9	2	2
unobserved		48.8	unobserved			106.8	unobserved		0.8	unobserved	2
50.9	0.01	50.9	93.0		ENDF	93.000	4.1	0.1	4.2	3	3
51.7	0.003	51.8	120.3	6.5		113.000	25.5	0.4	25.2	2	2
52.2	0.02	52.2	106.8		ENDF	106.800	1.4	0.1	1.4	3	3
55.2	0.005	55.2	111.0		ENDF	111.000	10.1	0.2	11.2	2	2
59.6	0.01	59.6	106.8		ENDF	106.800	6.2	0.2	6.6	2	2
61.4	0.01	61.4	141.0		ENDF	141.000	9.7	0.2	9.1	2	2
63.7	0.01	63.6	105.0		ENDF	105.000	4.4	0.1	4.5	3	3
67.6	0.1	67.6	106.8		ENDF	106.800	0.1	0.0	0.1	2	2
71.5	0.02	new	112.1		AVG	new	2.4	0.2	new	2	unassigned
73.2	0.01	73.2	106.8		ENDF	106.800	5.4	0.2	4.8	2	2
76.7	0.02	new	112.1		AVG	new	2.0	0.1	new	2	unassigned
77.2	0.02	77.1	106.8		ENDF	106.8	2.3	0.1	4.1	3	3
78.1	0.06	78.1	106.8		ENDF	106.8	0.5	0.0	0.5	3	3
82.3	0.01	82.3	106.8		ENDF	106.8	3.9	0.2	3.1	2	2
85.1	0.01	85.1	106.8		ENDF	106.8	5.5	0.2	5.1	3	3
88.8	0.01	88.8	106.0		ENDF	106.0	13.2	0.3	12.0	3	3
91.1	0.04	91.1	106.8		ENDF	106.8	1.3	0.1	1.4	2	2
93.3	0.005	93.3	110.0		ENDF	110.000	23.4	0.5	19.7	3	3
95.2	0.02	95.2	106.8		ENDF	106.8	2.5	0.1	2.8	3	3
101.4	0.01	101.4	96.0		ENDF	96.0	15.2	0.5	17.4	2	2
102.4	0.08	102.4	106.8		ENDF	106.8	0.7	0.1	0.7	2	2
104.2	0.07	104.1	106.8		ENDF	106.8	0.6	0.1	0.6	3	3
105.1	0.01	105.0	106.8		ENDF	106.8	7.3	0.3	8.0	2	2
110.5	0.01	110.5	106.8		ENDF	106.8	9.6	0.3	8.7	3	3
112.4	0.01	112.4	106.8		ENDF	106.8	11.6	0.4	11.4	2	2
113.4	0.03	113.4	106.8		ENDF	106.8	2.3	0.2	2.0	2	2
118.5	0.01	118.4	106.8		ENDF	106.8	8.6	0.4	8.9	2	2
120.6	0.01	120.5	106.8		ENDF	106.8	8.7	0.4	8.6	2	2
124.7	0.01	124.7	119.4	9.6	FIT	107.0	72.5	2.4	68.4	2	2

Table 6. Continued.

E_0 [eV]			Γ_γ [meV]				Γ_n [meV]			J value	
$E_{0,\mathrm{RPI}}$	$\Delta E_{0,\mathrm{RPI}}$	$E_{0,\mathrm{ENDF}}$	$\Gamma_{\gamma,\mathrm{RPI}}$	$\Delta\Gamma_{\gamma,\mathrm{RPI}}$	Γ_γ source	$\Gamma_{\gamma,\mathrm{ENDF}}$	$\Gamma_{n,\mathrm{RPI}}$	$\Delta\Gamma_{n,\mathrm{RPI}}$	$\Gamma_{n,\mathrm{ENDF}}$	RPI	ENDF
127.6	0.04	127.5	106.8		ENDF	106.8	2.1	0.2	2.5	3	3
131.2	0.02	131.2	106.8		ENDF	106.8	6.5	0.3	6.5	3	3
138.0	0.05	new	112.1		AVG	new	3.3	0.3	new	2	unassigned
138.5	0.01	138.4	120.0		ENDF	120.0	13.7	0.5	15.4	3	3
142.9	0.02	142.8	106.8		ENDF	106.8	11.6	0.5	11.2	2	2
144.8	0.03	144.8	106.8		ENDF	106.8	4.5	0.3	4.7	2	2
149.4	0.03	149.4	106.8		ENDF	106.8	3.2	0.2	3.2	3	3
153.9	0.02	153.8	106.8		ENDF	106.8	10.9	0.5	10.4	2	2
155.1	0.06	new	112.1		AVG	new	2.7	0.2	new	2	unassigned
156.9	0.02	156.8	106.8		ENDF	106.8	7.4	0.4	7.6	2	2
162.7	0.01	162.6	122.3	10.4	FIT	117.0	43.8	1.4	43.7	3	3
165.9	0.04	new	112.1		AVG	new	3.4	0.3	new	3	unassigned
166.6	0.01	166.6	112.5	10.5	FIT	115.0	40.9	1.6	45.6	2	2
168.7	0.01	168.6	110.6	9.4	FIT	110.0	84.7	3.3	78.0	2	2
170.2	0.02	170.1	106.8		ENDF	106.8	9.7	0.5	9.1	2	2
172.9	0.01	172.8	106.8		ENDF	106.8	13.5	0.5	14.6	3	3
175.3	0.02	175.3	106.8		ENDF	106.8	12.8	0.5	12.0	3	3
176.3	0.03	176.5	106.8		ENDF	106.8	8.0	0.5	12.9	3	3
177.0	0.04	new	112.1		AVG	new	7.4	0.6	new	2	unassigned
179.1	0.01	179.1	110.0		ENDF	110.0	20.7	0.7	20.6	3	3
183.8	0.01	183.7	108.5	10.6	FIT	106.8	22.5	0.9	35.1	3	3
184.5	0.04	new	112.1		AVG	new	7.2	0.6	new	2	unassigned
189.4	0.01	189.3	116.0	11.3	FIT	106.8	35.2	1.5	33.6	2	2
191.1	0.03	191.0	106.8		ENDF	106.8	7.0	0.5	7.0	2	2
193.1	0.10	192.9	106.8		ENDF	106.8	1.8	0.2	1.6	2	2
194.5	0.01	194.4	106.8		ENDF	106.8	17.6	0.7	17.1	3	3
197.4	0.02	197.3	102.5	9.9	FIT	105.0	24.4	1.1	24.6	2	2
203.0	0.02	202.8	109.3	10.5	FIT	106.8	27.8	1.4	26.3	2	2
206.1	0.01	206.0	122.7	11.8	FIT	120.0	38.0	1.5	43.2	2	2
208.6	0.04	208.5	106.8		ENDF	106.8	10.9	0.7	12.8	2	2
209.4	0.1	new	112.1		AVG	new	3.1	0.3	new	2	unassigned
210.6	0.01	210.5	104.9	10.1	FIT	106.8	33.1	1.6	31.2	2	2
212.1	0.02	212.0	106.8		ENDF	106.8	12.3	0.6	12.0	3	3
214.2	0.01	214.2	112.1	11.2	FIT	105.0	28.1	1.0	34.3	3	3
224.4	0.1	224.4	106.8		ENDF	106.8	5.2	0.4	5.4	2	2
227.9	0.02	227.8	108.2	10.5	FIT	106.8	22.8	1.0	22.3	3	3
235.5	0.02	235.5	107.0	10.7	FIT	106.8	23.9	1.2	36.0	2	2
236.5	0.1	new	112.1		AVG	new	6.1	0.5	new	2	unassigned
239.2	0.1	239.0	106.8		ENDF	106.8	3.7	0.3	3.7	3	3
240.9	0.1	240.8	106.8		ENDF	106.8	5.4	0.4	5.3	2	2
242.6	0.02	242.4	106.8		ENDF	106.8	13.1	0.7	12.9	3	3
245.3	0.02	245.3	109.8	10.8	FIT	106.8	23.4	1.1	22.3	3	3
251.7	0.1	251.8	106.8		ENDF	106.8	3.7	0.3	3.6	2	2
256.8	0.1	256.8	106.8		ENDF	106.8	2.2	0.2	2.0	2	2
258.9	0.04	258.7	106.8		ENDF	106.8	9.1	0.6	9.4	3	3

Table 6. Continued.

E_0 [eV]			Γ_γ [meV]				Γ_n [meV]			J value	
$E_{0,\mathrm{RPI}}$	$\Delta E_{0,\mathrm{RPI}}$	$E_{0,\mathrm{ENDF}}$	$\Gamma_{\gamma,\mathrm{RPI}}$	$\Delta\Gamma_{\gamma,\mathrm{RPI}}$	Γ_γ source	$\Gamma_{\gamma,\mathrm{ENDF}}$	$\Gamma_{n,\mathrm{RPI}}$	$\Delta\Gamma_{n,\mathrm{RPI}}$	$\Gamma_{n,\mathrm{ENDF}}$	RPI	ENDF
261.3	0.03	261.1	112.2	11.2	FIT	106.8	26.4	1.6	23.6	2	2
263.9	0.01	263.7	133.8	12.1	FIT	106.8	116.4	6.7	81.6	2	2
265.7	0.03	265.6	106.8		ENDF	106.8	17.3	1.1	16.8	2	2
268.0	0.1	267.8	106.8		ENDF	106.8	5.9	0.4	7.0	3	3
274.5	0.04	new	112.1		AVG	new	17.4	1.2	new	2	unassigned
275.8	0.02	275.7	101.9	9.6	FIT	118.0	51.2	2.5	85.7	3	3
283.7	0.07	283.6	106.8		ENDF	106.8	5.1	0.4	5.5	3	3
287.6	0.1	287.6	106.8		ENDF	106.8	3.6	0.3	3.5	3	3
288.6	0.1	new	112.1		AVG	new	2.5	0.2	new	3	unassigned
292.1	0.1	291.9	106.8		ENDF	106.8	4.7	0.4	4.9	2	2
293.9	0.04	293.6	106.8		ENDF	106.8	10.5	0.7	10.3	3	3
295.7	0.1	295.0	106.8		ENDF	106.8	3.0	0.3	2.9	2	2
300.1	0.02	299.9	112.8	11.3	FIT	106.8	31.2	1.5	32.6	3	3
302.5	0.1	302.4	106.8		ENDF	106.8	3.9	0.3	3.9	3	3
305.5	0.02	305.5	115.7	11.9	FIT	106.8	65.9	2.9	80.6	3	3
311.9	0.03	311.8	111.3	11.2	FIT	106.8	23.9	1.3	24.0	3	3
314.8	0.03	314.8	110.1	10.9	FIT	106.8	38.5	2.3	38.4	2	2
316.1	0.04	315.8	106.8		ENDF	106.8	15.8	1.0	13.7	3	3
319.9	0.02	319.6	137.8	13.4	FIT	135.0	46.5	2.5	44.4	2	2
328.7	0.2	328.7	106.8		ENDF	106.8	2.5	0.2	2.4	3	3
331.5	0.1	331.3	106.8		ENDF	106.8	7.6	0.7	7.4	2	2
338.1	0.02	337.6	171.9	9.4	FIT	130.0	364.3	28.4	252.0	2	2
343.6	0.04	343.5	105.8	10.5	FIT	106.8	27.4	1.8	31.2	2	2
349.7	0.1	349.5	106.8		ENDF	106.8	5.7	0.5	5.5	3	3
362.2	0.02	362.0	137.2	10.8	FIT	120.0	171.2	13.2	156.0	2	2
378.5	0.2	378.7	106.8		ENDF	106.8	3.3	0.3	3.3	3	3
381.2	0.1	381.2	106.8		ENDF	106.8	11.2	1.0	9.8	2	2
383.0	0.04	383.1	99.0	9.6	FIT	106.8	43.0	2.5	63.4	3	3
384.2	0.1	new	112.1		AVG	new	15.1	1.3	new	2	unassigned
389.4	0.1	388.9	106.8		ENDF	106.8	4.6	0.5	4.4	3	3
392.7	0.03	392.4	124.5	12.3	FIT	120.0	51.5	3.0	54.0	3	3
396.5	0.04	396.4	97.0	9.6	FIT	98.0	27.1	1.7	30.0	3	3
400.5	0.3	400.1	106.8		ENDF	106.8	2.0	0.2	2.0	2	2
403.1	0.2	402.9	106.8		ENDF	106.8	4.7	0.5	4.6	2	2
404.0	0.2	404.1	106.8		ENDF	106.8	2.6	0.3	2.6	3	3
415.6	0.04	415.3	107.3	10.6	FIT	106.8	40.5	2.8	43.2	2	2
420.2	0.05	420.0	106.8		ENDF	106.8	20.5	1.5	18.9	3	3
425.0	0.03	424.8	128.1	12.0	FIT	106.8	110.8	8.1	88.8	2	2
428.4	0.04	428.2	108.6	10.7	FIT	106.8	39.6	2.4	42.9	3	3
432.7	0.1	432.5	106.8		ENDF	106.8	10.3	0.8	10.3	3	3
435.2	0.1	435.1	106.8		ENDF	106.8	17.6	1.4	19.2	2	2
439.0	0.2	438.5	106.8		ENDF	106.8	5.9	0.6	6.0	2	2
440.3	0.2	440.1	106.8		ENDF	106.8	5.9	0.6	6.0	2	2
442.5	0.1	442.6	106.8		ENDF	106.8	8.7	0.7	9.4	3	3
444.0	0.2	new	112.1		AVG	new	5.4	0.5	new	3	unassigned

Table 6. Continued.

E_0 [eV]			Γ_γ [meV]				Γ_n [meV]			J value	
$E_{0,\mathrm{RPI}}$	$\Delta E_{0,\mathrm{RPI}}$	$E_{0,\mathrm{ENDF}}$	$\Gamma_{\gamma,\mathrm{RPI}}$	$\Delta\Gamma_{\gamma,\mathrm{RPI}}$	Γ_γ source	$\Gamma_{\gamma,\mathrm{ENDF}}$	$\Gamma_{n,\mathrm{RPI}}$	$\Delta\Gamma_{n,\mathrm{RPI}}$	$\Gamma_{n,\mathrm{ENDF}}$	RPI	ENDF
445.5	0.1	445.2	105.7	10.5	FIT	106.8	29.4	1.9	30.9	3	3
448.0	0.06	447.7	106.8	10.6	FIT	106.8	31.1	2.3	33.6	2	2
450.6	0.07	450.2	106.8	10.6	FIT	106.8	26.4	2.0	27.4	3	3
455.0	0.09	454.9	106.8		ENDF	106.8	18.2	1.5	18.0	2	2
459.3	0.04	458.9	117.4	11.5	FIT	106.8	62.0	4.8	52.8	2	2
462.7	0.04	462.4	119.1	11.0	FIT	106.8	100.0	7.8	87.6	2	2
472.6	0.05	472.3	110.8	10.9	FIT	106.8	50.2	4.0	45.6	2	2
474.4	0.13	new	112.1		AVG	new	16.4	1.4	new	2	unassigned
475.9	0.06	475.7	104.9	10.1	FIT	106.8	50.6	3.6	55.7	3	3
477.8	0.04	477.4	109.8	10.0	FIT	106.8	85.9	6.0	82.3	3	3
482.8	0.20	483.1	106.8		ENDF	106.8	9.1	0.8	9.5	2	2
unobserved		485.3				106.8			2.4	unobserved	3
490.0	0.05	490.6	106.8		ENDF	106.8	5.0	0.5	5.0	2	2
497.7	0.06	497.2	118.2	11.8	FIT	106.8	29.9	2.1	29.1	3	3
501.3	0.15	500.6	106.8		ENDF	106.8	6.0	0.6	6.6	3	3
504.1	0.11	503.6	106.8		ENDF	106.8	13.5	1.1	13.7	3	3
505.5	0.11	505.0	106.8		ENDF	106.8	15.7	1.3	12.0	3	3
507.1	0.07	506.8	112.9	11.2	FIT	106.8	33.9	2.6	31.2	2	2
511.9	0.19	new	112.1		AVG	new	7.3	0.7	new	2	unassigned
514.5	0.06	514.0	111.6	10.8	FIT	106.8	52.4	4.0	48.0	2	2
517.6	0.07	517.2	104.1	10.3	FIT	106.8	37.2	3.0	45.6	2	2
519.9	0.06	519.6	113.2	11.2	FIT	106.8	42.2	3.2	38.4	2	2
527.4	0.08	526.9	104.0	10.3	FIT	106.8	29.2	2.3	28.8	2	2
530.6	0.12	529.8	106.8		ENDF	106.8	15.0	1.4	12.7	2	2
535.5	0.06	535.1	118.4	11.5	FIT	106.8	58.5	4.6	45.6	2	2
539.7	0.08	539.6	93.6	9.2	FIT	106.8	37.8	3.2	57.6	2	2
540.8	0.13	new	112.1		AVG	new	18.9	1.7	new	2	unassigned
543.6	0.21	543.5	106.8		ENDF	106.8	7.9	0.8	6.2	2	2
545.5	0.07	545.4	109.3	10.9	FIT	106.8	25.4	1.9	30.9	3	3
553.1	0.09	553.0	106.8		ENDF	106.8	19.4	1.6	18.9	3	3
555.2	0.21	555.0	106.8		ENDF	106.8	5.7	0.5	6.1	3	3
559.8	0.19	559.5	106.8		ENDF	106.8	3.6	0.4	3.4	3	3
562.4	0.06	562.1	107.2	10.4	FIT	106.8	60.9	5.0	60.0	2	2
566.5	0.08	566.1	104.4	10.3	FIT	106.8	26.3	1.9	27.4	3	3
unobserved		574.7				106.8			2.9	unobserved	3
582.0	0.06	581.6	106.3	9.8	FIT	106.8	60.8	4.1	61.7	3	3
584.9	0.20	584.5	106.8		ENDF	106.8	12.1	1.1	12.0	2	2
unobserved		587.2				106.8			2.6	unobserved	3
591.4	0.35	591.2	106.8		ENDF	106.8	2.8	0.3	2.7	3	3
594.5	0.15	594.4	106.8		ENDF	106.8	12.6	1.2	12.0	3	3
596.1	0.06	595.6	106.8		ENDF	106.8	10.4	1.0	10.3	3	3
599.9	0.05	599.6	121.3	9.3	FIT	106.8	217.9	20.5	192.0	2	2
602.6	0.22	602.2	106.8		ENDF	106.8	9.6	0.9	9.5	2	2
608.7	0.17	607.6	106.8		ENDF	106.8	11.4	1.0	11.1	3	3
614.9	0.07	614.4	102.4	9.5	FIT	106.8	75.0	6.3	79.2	2	2

Table 6. Continued.

E_0 [eV]			Γ_γ [meV]				Γ_n [meV]			J value	
$E_{0,\mathrm{RPI}}$	$\Delta E_{0,\mathrm{RPI}}$	$E_{0,\mathrm{ENDF}}$	$\Gamma_{\gamma,\mathrm{RPI}}$	$\Delta\Gamma_{\gamma,\mathrm{RPI}}$	Γ_γ source	$\Gamma_{\gamma,\mathrm{ENDF}}$	$\Gamma_{n,\mathrm{RPI}}$	$\Delta\Gamma_{n,\mathrm{RPI}}$	$\Gamma_{n,\mathrm{ENDF}}$	RPI	ENDF
619.6	0.23	new	112.1		AVG	new	13.7	1.3	new	2	unassigned
620.9	0.07	620.3	104.1	9.9	FIT	106.8	64.8	5.1	68.6	3	3
625.2	0.19	624.9	106.8		ENDF	106.8	12.1	1.2	12.0	2	2
630.3	0.11	630.0	107.5	10.7	FIT	106.8	22.0	1.8	22.3	3	3
633.3	0.35	632.8	106.8		ENDF	106.8	7.5	0.7	7.4	3	3
633.6	0.36	new	112.1		AVG	new	10.4	1.0	new	2	unassigned
635.8	0.21	635.3	106.8		ENDF	106.8	15.0	1.4	14.4	2	2
636.7	0.27	new	112.1		AVG	new	9.1	0.9		2	unassigned
642.2	0.07	641.8	110.0	10.4	FIT	106.8	113.2	10.4	108.0	2	2
645.5	0.07	645.2	111.9	10.7	FIT	106.8	90.5	8.0	84.0	2	2
648.8	0.12	648.6	106.8		ENDF	106.8	20.7	1.7	20.6	3	3
651.2	0.05	652.0	106.8		ENDF	106.8	9.0	0.9	9.2	2	2
657.7	0.34	657.1	106.8		ENDF	106.8	6.0	0.6	6.0	2	2
666.0	0.40	665.0	106.8		ENDF	106.8	3.2	0.3	3.1	3	3
671.0	0.06	670.5	108.3	9.4	FIT	106.8	113.3	9.9	111.4	3	3
672.8	0.09	672.2	117.0	11.4	FIT	106.8	76.6	6.9	67.2	2	2
675.3	0.25	674.9	106.8		ENDF	106.8	8.2	0.8	8.1	3	3
678.0	0.27	677.6	106.8		ENDF	106.8	7.0	0.7	6.7	3	3
680.8	0.08	680.7	109.7	10.6	FIT	106.8	91.1	8.0	87.6	2	2
682.3	0.17	new	112.1		AVG	new	26.1	2.4	new	2	unassigned
687.3	0.16	new	112.1		AVG	new	10.4	1.0	new	2	unassigned
692.3	0.03	691.9	107.1	10.6	FIT	106.8	42.9	4.0	43.2	2	2
697.5	0.10	697.3	110.8	11.0	FIT	106.8	40.3	3.4	36.9	3	3
699.6	0.15	698.9	106.8		ENDF	106.8	18.5	1.7	17.1	3	3
704.4	0.36	704.5	106.8		ENDF	106.8	7.0	0.7	7.0	2	2
710.2	0.45	709.3	106.8		ENDF	106.8	3.2	0.3	3.1	3	3
713.1	0.16	712.9	108.1	10.9	FIT	106.8	30.3	3.0	28.8	2	2
715.3	0.10	714.8	114.9	11.4	FIT	106.8	92.2	8.8	84.0	2	2
717.3	0.34	new	112.1		AVG	new	13.0	1.3	new	2	unassigned
719.1	0.25	new	112.1		AVG	new	11.1	1.1	new	3	unassigned
721.5	0.08	720.9	110.4	10.9	FIT	106.8	53.5	4.5	50.6	3	3
724.8	0.13	724.3	106.8		ENDF	106.8	20.4	1.9	18.9	3	3
730.0	0.11	729.7	109.3	10.8	FIT	106.8	55.0	4.8	52.8	2	2
736.7	0.12	736.2	111.4	11.1	FIT	106.8	62.3	5.8	57.6	2	2
739.1	0.10	738.2	110.0	10.8	FIT	106.8	95.0	8.9	91.2	2	2
741.3	0.16	740.4	108.0	10.8	FIT	106.8	34.9	3.3	33.6	2	2
744.2	0.14	743.9	106.1	10.6	FIT	106.8	25.2	2.2	25.7	3	3
747.0	0.11	746.6	108.1	10.8	FIT	106.8	35.4	3.0	34.3	3	3
750.4	0.12	750.0	108.3	10.7	FIT	106.8	41.9	3.7	40.8	2	2
756.4	0.34	755.5	106.8		ENDF	106.8	10.0	1.0	10.0	2	2
759.8	0.3	759.6	106.8		ENDF	106.8	14.5	1.4	14.4	2	2
763.9	0.3	763.7	106.8		ENDF	106.8	11.2	1.1	11.1	3	3
767.1	0.3	766.6	106.8		ENDF	106.8	10.9	1.1	11.1	3	3
771.4	0.2	770.8	110.6	11.0	FIT	106.8	25.9	2.3	24.9	3	3
773.8	0.1	773.7	108.0	10.7	FIT	106.8	51.8	4.8	50.4	2	2

Table 6. Continued.

E_0 [eV]			Γ_γ [meV]				Γ_n [meV]			J value	
$E_{0,\mathrm{RPI}}$	$\Delta E_{0,\mathrm{RPI}}$	$E_{0,\mathrm{ENDF}}$	$\Gamma_{\gamma,\mathrm{RPI}}$	$\Delta\Gamma_{\gamma,\mathrm{RPI}}$	Γ_γ source	$\Gamma_{\gamma,\mathrm{ENDF}}$	$\Gamma_{n,\mathrm{RPI}}$	$\Delta\Gamma_{n,\mathrm{RPI}}$	$\Gamma_{n,\mathrm{ENDF}}$	RPI	ENDF
775.7	0.3	new	112.1		AVG	new	23.3	2.2	new	2	unassigned
777.4	0.1	776.3	108.7	10.3	FIT	106.8	95.3	8.6	93.6	2	2
780.7	0.1	780.1	123.3	11.1	FIT	106.8	215.9	20.3	192.0	2	2
784.6	0.1	784.1	106.5	10.5	FIT	106.8	39.3	3.3	39.4	3	3
787.1	0.3	786.6	106.8		ENDF	106.8	13.0	1.2	12.9	3	3
790.8	0.4	791.0	106.8		ENDF	106.8	7.4	0.7	7.2	2	2
798.5	0.1	797.5	106.8		ENDF	106.8	8.6	0.9	8.6	3	3
unobserved		803.9				106.8			4.8	unobserved	2
808.2	0.2	807.7	106.8		ENDF	106.8	16.7	1.6	16.3	3	3
810.0	0.3	new	112.1		AVG	new	16.6	1.6	new	2	unassigned
813.1	0.1	812.8	105.5	10.3	FIT	106.8	46.4	3.9	48.0	3	3
815.1	0.2	new	112.1		AVG	new	23.0	2.1	new	3	unassigned
818.2	0.3	818.1	106.8		ENDF	106.8	10.5	1.0	10.3	3	3
820.7	0.4	821.0	106.8		ENDF	106.8	11.9	1.2	12.0	2	2
831.9	0.1	831.4	105.2	10.3	FIT	106.8	63.1	5.8	64.8	2	2
833.7	0.0	834.0	106.8		ENDF	106.8	14.4	1.4	14.6	3	3
836.4	0.1	836.1	105.8	9.8	FIT	106.8	78.2	6.7	79.7	3	3
845.3	0.3	845.6	106.8		ENDF	106.8	13.3	1.3	13.7	3	3
851.1	0.2	850.6	105.4	10.4	FIT	106.8	34.2	3.0	36.0	3	3
856.4	0.2	856.1	106.8		ENDF	106.8	21.5	2.0	20.6	3	3
860.7	0.1	860.5	113.1	10.6	FIT	106.8	81.9	6.8	75.4	3	3
864.4	0.2	864.1	106.9	10.7	FIT	106.8	21.9	2.1	22.3	3	3
867.8	0.2	867.2	111.0	11.3	FIT	106.8	33.2	3.4	28.8	2	2
879.1	0.4	879.0	106.8		ENDF	106.8	10.9	1.1	10.8	2	2
882.1	0.1	881.6	107.8	9.6	FIT	106.8	171.1	16.3	168.0	2	2
885.7	0.2	885.3	107.9	10.6	FIT	106.8	43.5	3.8	42.9	3	3
893.3	0.3	892.9	107.1	10.7	FIT	106.8	23.0	2.2	22.8	2	2
897.0	0.1	897.0	106.8		ENDF	106.8	8.7	0.9	8.6	2	2
900.1	0.3	900.0	106.8		ENDF	106.8	12.3	1.2	12.0	3	3
903.6	0.0	903.2	107.0	10.6	FIT	106.8	56.1	5.4	56.6	3	3
908.6	0.4	new	112.1		AVG	new	12.6	1.2	new	3	unassigned
910.8	0.2	910.2	107.7	10.8	FIT	106.8	38.4	3.6	37.7	3	3
915.2	0.1	914.3	115.6	10.1	FIT	106.8	176.8	16.1	162.9	3	3
918.5	0.1	918.1	107.7	10.3	FIT	106.8	109.8	10.3	108.0	2	2
923.1	0.3	922.9	106.8		ENDF	106.8	16.0	1.6	15.4	3	3
926.0	0.2	925.5	111.7	11.1	FIT	106.8	93.7	9.0	87.6	2	2
934.4	0.1	933.2	106.8		ENDF	106.8	20.6	2.0	20.6	3	3
941.8	0.1	941.1	106.8		ENDF	106.8	14.4	1.4	14.4	2	2
943.6	0.2	943.0	107.0	10.6	FIT	106.8	62.6	5.9	62.4	2	2
946.3	0.3	new	112.1		AVG	new	25.6	2.4	new	3	unassigned
948.8	0.2	948.1	109.2	10.8	FIT	106.8	92.7	9.0	88.8	2	2
954.4	0.3	new	112.1		AVG	new	19.9	1.9	new	3	unassigned
956.6	0.4	955.3	107.3	10.8	FIT	106.8	29.3	2.9	28.8	2	2
959.0	0.2	958.2	107.4	10.6	FIT	106.8	59.0	5.3	58.3	3	3
963.7	0.4	963.2	106.8		ENDF	106.8	10.3	1.0	10.3	3	3

Table 6. Continued.

E_0 [eV]			Γ_γ [meV]				Γ_n [meV]			J value	
$E_{0,\mathrm{RPI}}$	$\Delta E_{0,\mathrm{RPI}}$	$E_{0,\mathrm{ENDF}}$	$\Gamma_{\gamma,\mathrm{RPI}}$	$\Delta\Gamma_{\gamma,\mathrm{RPI}}$	Γ_γ source	$\Gamma_{\gamma,\mathrm{ENDF}}$	$\Gamma_{n,\mathrm{RPI}}$	$\Delta\Gamma_{n,\mathrm{RPI}}$	$\Gamma_{n,\mathrm{ENDF}}$	RPI	ENDF
965.7	0.6	965.2	106.8		ENDF	106.8	7.7	0.8	7.7	3	3
972.9	0.2	972.2	112.5	11.4	FIT	106.8	96.3	9.6	90.0	2	2
976.3	0.2	975.7	108.1	10.9	FIT	106.8	34.1	3.4	32.6	3	3
978.8	0.1	978.5	105.4	9.9	FIT	106.8	101.1	9.3	102.9	3	3
981.2	0.1	980.9	106.8		ENDF	106.8	16.9	1.7	16.8	2	2
990.4	0.1	989.3	114.0	10.9	FIT	106.8	166.2	16.0	156.0	2	2
993.4	0.2	992.8	106.8		ENDF	106.8	11.3	1.1	11.1	3	3
995.7	0.0	996.2	106.8		ENDF	106.8	7.3	0.7	7.2	2	2

Table 7. Resonance parameters for ^{162}Dy isotopes compared with ENDF/B-VII.1.

E_0 [eV]			Γ_γ [meV]				Γ_n [meV]			J value	
$E_{0,\mathrm{RPI}}$	$\Delta E_{0,\mathrm{RPI}}$	$E_{0,\mathrm{ENDF}}$	$\Gamma_{\gamma,\mathrm{RPI}}$	$\Delta\Gamma_{\gamma,\mathrm{RPI}}$	Γ_γ source	$\Gamma_{\gamma,\mathrm{ENDF}}$	$\Gamma_{n,\mathrm{RPI}}$	$\Delta\Gamma_{n,\mathrm{RPI}}$	$\Gamma_{n,\mathrm{ENDF}}$	RPI	ENDF
71.1	0.004	71.1	86.0	3.5	FIT	125.0	448.8	5.6	400.0	0.5	0.5
117.2	0.007	117.2	120.0		ENDF	120.0	12.0	0.4	9.5	0.5	0.5
208.1	0.01	208.0	110.2	10.5	FIT	105.0	25.0	0.9	24.0	0.5	0.5
223.5	0.01	223.3	114.6	10.5	FIT	115.0	41.1	1.9	37.0	0.5	0.5
269.4	0.01	269.4	94.3	4.9	FIT	116.8	708.4	20.5	620.0	0.5	0.5
357.4	0.03	357.0	102.1	10.0	FIT	105.0	25.0	1.5	26.3	0.5	0.5
413.2	0.02	412.8	86.0	5.8	FIT	100.0	152.7	13.3	150.0	0.5	0.5
470.4	0.1	470.3	116.8		ENDF	116.8	9.0	0.8	8.0	0.5	0.5
530.0	0.03	529.8	70.2	3.9	FIT	120.0	314.6	29.9	280.0	0.5	0.5
633.0	0.1	632.8	89.8	5.4	FIT	116.8	1692.1	108.5	1510.0	0.5	0.5
686.4	0.05	686.0	96.2	5.5	FIT	110.0	486.2	44.8	445.0	0.5	0.5
717.1	0.1	716.5	100.5	5.6	FIT	130.0	613.8	54.7	590.0	0.5	0.5
766.8	0.1	766.4	87.3	5.3	FIT	116.8	861.5	73.1	860.0	0.5	0.5
866.8	0.1	866.0	103.8	7.3	FIT	116.8	2720.7	157.5	2500.0	0.5	0.5
951.6	0.02	952.1	71.4	6.0	FIT	110.0	186.2	17.3	194.0	0.5	0.5

Each experimental data set was plotted with the final parameters (fit without solving Bayes equations), and the reduced chi-squared values were generated from the SAMMY. The final reduced χ^2 values of ^{161}Dy, ^{162}Dy, ^{163}Dy, ^{164}Dy, and $^{\mathrm{nat}}$Dy capture yield were 1.03, 1.05, 1.04, 1.06, and 1.07, respectively and the final reduced χ^2 values of $^{\mathrm{nat}}$Dy transmission was 1.22. The reason for the near unity χ^2 are the relatively large uncertainties on the capture yield of the isotopic samples.

The resonance integrals (RI) from the present resonance parameters are compared with those of ENDF/B-VII.1 in table 10. The RIs for each dysprosium isotope were calculated from 0.5 eV to 20 MeV with the same method used in Kang *et al.* [17] using the NJOY code [25] and INTER code [26]. The RI uncertainties in table 10 were determined with Barry's method suggested in his thesis [21]. This method used resonance parameter error propagation on the simple Breit-Wigner formula. The RI of ^{160}Dy is 21% larger than the RI from resonance parameters of ENDF/B-VII.1. The percent change of the RI for the other isotopes are within 2% of the ENDF/B-VII.1 values. A RI value of the natural dysprosium calculated with present resonance parameters was 1405 ± 3.5 barn. The value is $\sim 0.3\%$ higher than that obtained with the ENDF/B-VII.1 parameters.

Table 8. Resonance parameters for ^{163}Dy isotopes compared with ENDF/B-VII.1.

E_0 [eV]			Γ_γ [meV]				Γ_n [meV]			J value	
$E_{0,\mathrm{RPI}}$	$\Delta E_{0,\mathrm{RPI}}$	$E_{0,\mathrm{ENDF}}$	$\Gamma_{\gamma,\mathrm{RPI}}$	$\Delta\Gamma_{\gamma,\mathrm{RPI}}$	Γ_γ source	$\Gamma_{\gamma,\mathrm{ENDF}}$	$\Gamma_{n,\mathrm{RPI}}$	$\Delta\Gamma_{n,\mathrm{RPI}}$	$\Gamma_{n,\mathrm{ENDF}}$	RPI	ENDF
16.2	0.001	16.2	105.0		ENDF	105.0	21.8	0.2	18.3	−3	−3
19.7	0.01	19.7	108.6		ENDF	108.6	0.8	0.0	0.9	−3	−3
35.8	0.002	35.8	108.6		ENDF	108.6	13.5	0.2	9.8	−2	−2
50.3	0.01	50.3	108.6		ENDF	108.6	3.3	0.1	2.8	−3	−3
55.9	0.002	55.9	137.5	4.9	FIT	120.0	26.8	0.4	24.0	−3	−3
59.1	0.003	59.0	106.2	4.9	FIT	111.0	105.0	2.2	98.4	−2	−2
66.1	0.005	66.1	108.6		ENDF	108.6	8.5	0.2	7.2	−3	−3
72.0	0.01	72.0	108.6		ENDF	108.6	4.4	0.2	4.2	−2	−2
75.4	0.01	75.5	108.6		ENDF	108.6	3.6	0.2	2.8	−2	−2
79.0	0.005	79.0	108.6		ENDF	108.6	20.8	0.5	17.4	−2	−2
86.3	0.03	86.3	108.6		ENDF	108.6	1.3	0.1	1.0	−3	−3
94.1	0.01	94.1	108.6		ENDF	108.6	19.4	0.4	17.1	−3	−3
105.9	0.004	105.9	119.6	7.9	FIT	108.6	65.8	1.5	54.0	−3	−3
107.2	0.01	107.2	110.1	8.4	FIT	108.6	39.4	0.9	33.6	−2	−2
120.4	0.01	120.3	108.6		ENDF	108.6	9.7	0.4	8.2	−3	−3
126.6	0.01	126.6	108.6		ENDF	108.6	16.8	0.5	15.3	−3	−3
127.5	0.01	127.5	108.6		ENDF	108.6	13.2	0.4	11.2	−3	−3
135.4	0.02	135.3	108.6		ENDF	108.6	5.7	0.3	4.5	−3	−3
143.5	0.01	143.4	108.6		ENDF	108.6	16.8	0.7	20.4	−2	−2
145.0	0.01	145.0	103.6	9.1	FIT	100.0	54.3	1.9	55.2	−2	−2
155.1	0.01	155.0	100.1	8.0	FIT	110.0	105.9	6.7	99.6	−2	−2
163.9	0.01	163.8	108.6		ENDF	108.6	11.2	0.5	10.3	−3	−3
177.2	0.04	177.2	108.6		ENDF	108.6	3.7	0.3	3.4	−3	−3
185.2	0.03	185.1	108.6		ENDF	108.6	4.4	0.3	4.6	−3	−3
189.0	0.05	189.0	108.6		ENDF	108.6	4.2	0.3	4.1	−2	−2
203.0	0.02	202.9	106.0	10.2	FIT	108.6	22.2	1.1	25.2	−2	−2
205.4	0.01	205.3	100.4	9.1	FIT	95.0	54.2	2.2	46.3	−3	−3
213.8	0.03	213.7	108.6		ENDF	108.6	6.4	0.4	5.7	−3	−3
223.9	0.02	224.2	101.5	6.9	FIT	160.0	189.7	15.1	216.0	−2	−2
224.6	0.02	new	108.3		AVG	new	30.1	2.3	new	−3	unassigned
233.7	0.04	233.5	108.6		ENDF	108.6	6.2	0.4	6.3	−3	−3
250.7	0.02	250.6	108.6		ENDF	108.6	15.6	0.8	15.4	−3	−3
261.3	0.01	261.1	99.8	7.8	FIT	87.0	107.3	7.8	91.7	−3	−3
268.2	0.01	268.0	98.9	7.3	FIT	90.0	133.1	9.6	120.0	−3	−3
274.4	0.02	274.2	115.9	11.4	FIT	108.6	37.5	2.1	33.6	−2	−2
281.2	0.02	281.1	110.5	10.8	FIT	108.6	27.8	1.4	26.6	−3	−3
289.1	0.02	288.9	94.9	6.2	FIT	130.0	145.2	11.9	151.2	−2	−2
295.9	0.07	296.0	108.6		ENDF	108.6	7.9	0.7	7.1	−2	−2
297.3	0.07	new	108.3		AVG	new	13.0	1.2	new	−2	unassigned
298.1	0.02	297.8	92.8	7.6	FIT	108.6	92.6	6.8	103.2	−2	−2
unobserved		307.1				108.6			1.9	unobserved	−2
323.1	0.02	323.1	103.8	5.5	FIT	128.0	252.8	22.3	240.0	−3	−3
324.7	0.02	324.6	101.1	6.9	FIT	100.0	257.4	19.8	231.4	−3	−3
327.2	0.03	326.9	108.7	10.9	FIT	108.6	34.0	2.0	42.1	−2	−2

Table 8. Continued.

E_0 [eV]			Γ_γ [meV]				Γ_n [meV]			J value	
$E_{0,\mathrm{RPI}}$	$\Delta E_{0,\mathrm{RPI}}$	$E_{0,\mathrm{ENDF}}$	$\Gamma_{\gamma,\mathrm{RPI}}$	$\Delta\Gamma_{\gamma,\mathrm{RPI}}$	Γ_γ source	$\Gamma_{\gamma,\mathrm{ENDF}}$	$\Gamma_{n,\mathrm{RPI}}$	$\Delta\Gamma_{n,\mathrm{RPI}}$	$\Gamma_{n,\mathrm{ENDF}}$	RPI	ENDF
329.7	0.05	329.7	108.6		ENDF	108.6	19.3	1.3	20.4	−2	−2
343.1	0.04	342.9	108.6		ENDF	108.6	20.0	1.3	19.7	−3	−3
348.4	0.02	348.3	96.0	5.9	FIT	110.0	297.4	24.4	288.0	−2	−2
368.8	0.02	368.6	134.3	9.6	FIT	120.0	214.3	17.3	204.0	−2	−2
375.4	0.17	375.0	108.6		ENDF	108.6	3.3	0.3	3.3	−3	−3
382.4	0.07	382.2	108.6		ENDF	108.6	6.1	0.6	6.1	−2	−2
387.3	0.04	387.0	112.1	11.1	FIT	108.6	32.9	2.3	28.8	−2	−2
390.6	0.03	390.4	89.9	8.5	FIT	90.0	45.0	2.8	47.1	−3	−3
400.4	0.04	400.3	109.4	10.8	FIT	108.6	34.6	2.4	33.6	−2	−2
403.1	0.19	403.2	108.6		ENDF	108.6	4.0	0.4	4.1	−2	−2
411.4	0.02	411.1	176.0	8.9	FIT	155.0	626.9	40.1	648.0	−2	−2
420.8	0.23	420.6	108.6		ENDF	108.6	2.5	0.2	2.4	−3	−3
429.6	0.04	429.4	67.4	6.3	FIT	70.0	36.2	2.6	39.4	−3	−3
455.1	0.03	454.8	147.8	14.0	FIT	150.0	75.9	4.5	80.6	−3	−3
459.5	0.06	459.2	107.8	10.7	FIT	108.6	22.5	1.6	25.7	−3	−3
465.5	0.06	465.3	108.6		ENDF	108.6	20.7	1.5	18.9	−3	−3
479.4	0.04	479.1	148.6	13.8	FIT	150.0	85.1	6.1	84.0	−2	−2
484.0	0.04	483.6	120.1	11.0	FIT	120.0	94.7	6.9	94.8	−2	−2
502.7	0.15	new	108.3		AVG	new	9.3	0.8	new	−2	unassigned
504.5	0.11	new	108.3		AVG	new	22.5	2.1	new	−2	unassigned
505.2	0.05	504.6	62.1	5.1	FIT	80.0	126.9	12.1	144.0	−2	−2
516.5	0.06	516.3	114.0	11.3	FIT	108.6	25.8	1.9	25.7	−3	−3
519.4	0.11	519.8	101.2	10.1	FIT	108.6	19.5	1.7	26.4	−2	−2
520.4	0.13	new	108.3		AVG	new	14.1	1.3	new	−2	unassigned
533.6	0.04	533.2	122.2	8.5	FIT	130.0	248.3	22.2	240.0	−2	−2
542.7	0.03	542.2	125.3	8.8	FIT	135.0	342.2	28.4	288.0	−2	−2
564.6	0.06	564.3	87.4	7.9	FIT	85.0	76.7	6.5	74.4	−2	−2
569.4	0.03	569.0	157.1	13.7	FIT	150.0	157.6	12.7	148.8	−2	−2
581.1	0.05	580.8	126.3	11.8	FIT	130.0	73.2	5.5	75.4	−3	−3
594.8	0.05	594.5	112.3	10.3	FIT	108.6	86.7	6.9	84.0	−3	−3
601.5	0.04	601.3	143.9	12.4	FIT	130.0	199.3	16.6	180.0	−2	−2
616.2	0.1	615.7	73.1	6.6	FIT	75.0	57.3	4.6	60.0	−3	−3
621.0	0.1	620.8	122.4	11.0	FIT	110.0	134.4	12.1	120.0	−2	−2
632.7	0.1	632.1	95.8	7.2	FIT	125.0	155.1	13.9	180.0	−3	−3
637.6	0.1	637.2	135.7	11.4	FIT	135.0	196.4	17.5	192.0	−2	−2
642.4	0.1	642.0	77.4	6.3	FIT	100.0	112.1	9.3	137.1	−3	−3
646.8	0.0	646.3	151.1	14.3	FIT	150.0	102.1	7.1	102.9	−3	−3
652.6	0.3	652.2	108.6		ENDF	108.6	7.4	0.7	7.2	−2	−2
unobserved		660.4				108.6			22.8	unobserved	−2
666.8	0.1	new	108.3		AVG	new	49.5	4.2	new	−2	unassigned
685.2	0.3	new	108.3		AVG	new	6.6	0.6	new	−3	unassigned
687.6	0.1	687.0	108.6		ENDF	108.6	22.3	2.0	20.6	−3	−3
694.0	0.3	new	108.3		AVG	new	12.6	1.2	new	−2	unassigned
696.3	0.1	695.7	118.9	10.3	FIT	115.0	199.6	18.4	192.0	−2	−2

Table 8. Continued.

E_0 [eV]			Γ_γ [meV]				Γ_n [meV]			J value	
$E_{0,\mathrm{RPI}}$	$\Delta E_{0,\mathrm{RPI}}$	$E_{0,\mathrm{ENDF}}$	$\Gamma_{\gamma,\mathrm{RPI}}$	$\Delta\Gamma_{\gamma,\mathrm{RPI}}$	Γ_γ source	$\Gamma_{\gamma,\mathrm{ENDF}}$	$\Gamma_{n,\mathrm{RPI}}$	$\Delta\Gamma_{n,\mathrm{RPI}}$	$\Gamma_{n,\mathrm{ENDF}}$	RPI	ENDF
710.3	0.3	709.8	108.6		ENDF	108.6	10.1	1.0	9.6	−2	−2
712.8	0.1	712.5	94.3	8.8	FIT	95.0	90.4	8.3	90.0	−2	−2
714.1	0.2	new	108.3		AVG	new	20.8	2.0	new	−2	unassigned
721.7	0.1	721.3	75.2	7.0	FIT	75.0	73.1	6.3	73.7	−3	−3
732.4	0.1	732.1	108.6		ENDF	108.6	17.0	1.7	16.3	−3	−3
736.4	0.2	736.1	108.6		ENDF	108.6	17.4	1.6	17.1	−3	−3
742.4	0.2	741.7	108.6		ENDF	108.6	19.8	1.8	18.9	−3	−3
747.3	0.4	747.2	108.6		ENDF	108.6	8.4	0.8	8.4	−2	−2
756.4	0.1	756.1	82.4	8.0	FIT	85.0	41.7	3.6	44.6	−3	−3
758.5	0.3	new	108.3		AVG	new	13.2	1.3	new	−2	unassigned
764.5	0.2	764.3	108.6		ENDF	108.6	22.0	2.1	21.6	−2	−2
767.5	0.3	new	108.3		AVG	new	15.0	1.4	new	−2	unassigned
770.6	0.4	769.9	108.6		ENDF	108.6	5.8	0.6	5.7	−3	−3
776.7	0.2	776.6	108.0	10.8	FIT	108.6	24.3	2.2	24.0	−3	−3
794.5	0.1	794.4	110.0	10.9	FIT	108.6	47.5	4.2	46.3	−3	−3
796.1	0.2	new	108.3		AVG	new	23.1	2.2	new	−2	unassigned
810.2	0.1	809.5	138.5	11.2	FIT	108.6	362.3	36.6	312.0	−2	−2
813.2	0.1	812.3	117.8	11.9	FIT	108.6	69.7	6.8	60.0	−2	−2
823.4	0.1	823.0	109.3	10.9	FIT	108.6	41.9	3.7	41.1	−3	−3
831.6	0.1	830.9	109.6	10.3	FIT	108.6	105.4	9.7	104.4	−2	−2
834.9	0.3	new	108.3		AVG	new	11.4	1.1	new	−3	unassigned
845.9	0.2	846.6	108.6		ENDF	108.6	11.2	1.1	11.1	−3	−3
850.5	0.2	new	108.3		AVG	108.6	24.1	2.4	new	−2	unassigned
852.0	0.1	851.2	108.5	9.5	FIT	108.6	192.6	18.6	192.0	−2	−2
858.4	0.1	857.8	112.6	11.1	FIT	108.6	75.3	7.0	70.8	−2	−2
864.1	0.2	new	108.3		AVG	new	26.7	2.4	new	−3	unassigned
865.9	0.2	864.9	105.8	10.4	FIT	108.6	59.4	5.5	62.4	−2	−2
874.2	0.1	873.9	108.2	10.1	FIT	108.6	100.8	8.8	102.9	−3	−3
900.8	0.1	899.7	97.4	7.9	FIT	108.6	210.2	20.3	216.0	−2	−2
919.2	0.1	918.7	105.1	10.0	FIT	108.6	74.1	6.6	78.0	−3	−3
920.7	0.2	new	108.3		AVG	new	41.2	3.8	new	−3	unassigned
930.5	0.1	929.8	98.5	8.4	FIT	108.6	240.0	22.2	252.0	−2	−2
936.0	0.2	935.8	108.8	10.8	FIT	108.6	32.5	2.9	32.6	−3	−3
940.1	0.1	939.5	86.4	6.8	FIT	108.6	207.9	19.5	222.9	−3	−3
950.0	0.1	949.7	103.5	9.5	FIT	108.6	169.6	16.1	168.0	−2	−2
954.6	0.4	new	108.3		AVG	new	15.3	1.5	new	−2	unassigned
958.2	0.1	957.8	109.5	10.9	FIT	108.6	31.3	3.0	30.9	−3	−3
967.5	0.2	967.4	111.4	11.1	FIT	108.6	60.8	5.8	57.6	−2	−2
973.7	0.1	972.8	120.8	10.6	FIT	108.6	294.9	29.4	276.0	−2	−2
980.9	0.4	980.5	108.6		ENDF	108.6	11.3	1.1	11.1	−3	−3
997.3	0.2	996.6	109.8	10.9	FIT	108.6	66.3	6.3	64.8	−2	−2

Table 9. Resonance parameters for ^{164}Dy isotopes compared with ENDF/B-VII.1.

E_0 [eV]			Γ_γ [meV]				Γ_n [meV]			J value	
$E_{0,\mathrm{RPI}}$	$\Delta E_{0,\mathrm{RPI}}$	$E_{0,\mathrm{ENDF}}$	$\Gamma_{\gamma,\mathrm{RPI}}$	$\Delta\Gamma_{\gamma,\mathrm{RPI}}$	Γ_γ source	$\Gamma_{\gamma,\mathrm{ENDF}}$	$\Gamma_{n,\mathrm{RPI}}$	$\Delta\Gamma_{n,\mathrm{RPI}}$	$\Gamma_{n,\mathrm{ENDF}}$	RPI	ENDF
147.1	0.007	147.0	88.8	4.185	FIT	114.2	844.3	11.090	820.0	0.5	0.5
unobserved		227.6	unobserved			114.2	unobserved		0.4	unobserved	−0.5
450.5	0.036	450.4	72.8	4.144	FIT	110.0	268.2	24.310	260.0	0.5	0.5
unobserved		479.4	unobserved			114.2	unobserved		0.8	unobserved	−1.5
536.7	0.034	536.3	63.5	4.913	FIT	120.0	106.3	9.135	116.0	0.5	0.5
549.2	0.133	548.8	114.2		ENDF	114.2	6.9	0.612	6.8	0.5	0.5
unobserved		740.9	unobserved			114.2	unobserved		1.5	unobserved	−1.5
805.2	0.256	804.2	114.2		ENDF	114.2	9.1	0.870	8.8	−0.5	−0.5
854.4	0.072	853.9	82.4	5.143	FIT	114.2	514.4	48.650	550.0	0.5	0.5
unobserved		925.9	unobserved			114.2	unobserved		1.5	unobserved	−1.5
941.5	0.411	941.0	114.2		ENDF	114.2	2.4	0.241	2.5	−1.5	−1.5
983.7	0.094	983.1	110.4	9.757	FIT	120.0	105.8	8.808	120.0	0.5	0.5

Table 10. Calculated capture resonance integrals for dysprosium isotopes in the energy range from 0.5 eV to 20 MeV.

Isotope	Abundance [%]	Capture resonance integral [b]		Percent change [%]
		Present	ENDF/B-VII.1	
^{156}Dy	0.06	–	1021	–
^{158}Dy	0.1	–	247	–
^{160}Dy	2.34	1342 ± 24	1107	+21
^{161}Dy	18.9	1083 ± 14	1076	+0.6
^{162}Dy	25.5	2735 ± 3	2757	−0.8
^{163}Dy	24.9	1510 ± 8.4	1489	+1.4
^{164}Dy	28.2	338 ± 0.8	343	−1.8
$^{\mathrm{nat}}$Dy	–	1405 ± 3.5	1401	+0.3

5.2 Resonance parameter statistics

The missing level curves of each isotope were plotted by assuming the level spacing is theoretically a constant as shown in fig. 4. The average level spacing, D_0, is the inverse of the slope in the range judged that D_0 is constant. The D_0 for ^{160}Dy, ^{161}Dy, and ^{163}Dy seem to be constant up to 202.2, 120.6, and 163.9 eV, respectively. For ^{162}Dy and ^{164}Dy D_0 seems constant up to 1000 eV because they have few resonances. The D_0 for ^{160}Dy, ^{161}Dy, ^{162}Dy, ^{163}Dy, and ^{164}Dy are shown in table 11. The D_0 values of ^{160}Dy, ^{161}Dy, and ^{163}Dy are different from those of the Atlas [27] by $\sim$ 38%, $\sim$ 17%, and $\sim$ 5%, respectively. The uncertainties in D_0 given in table 11 for the current measurement are the uncertainties in the fitted slopes from fig. 4. The uncertainties in D_0 given in table 11 for the Atlas values are from Mughabghab [27]. According to the missing level curve shown in fig. 4, there exist about 24 missing levels for ^{160}Dy and about 130 missing levels for ^{161}Dy in the region up to 1000 eV. Table 11 and fig. 4 also provide comparison to the values from Mughabghab [27].

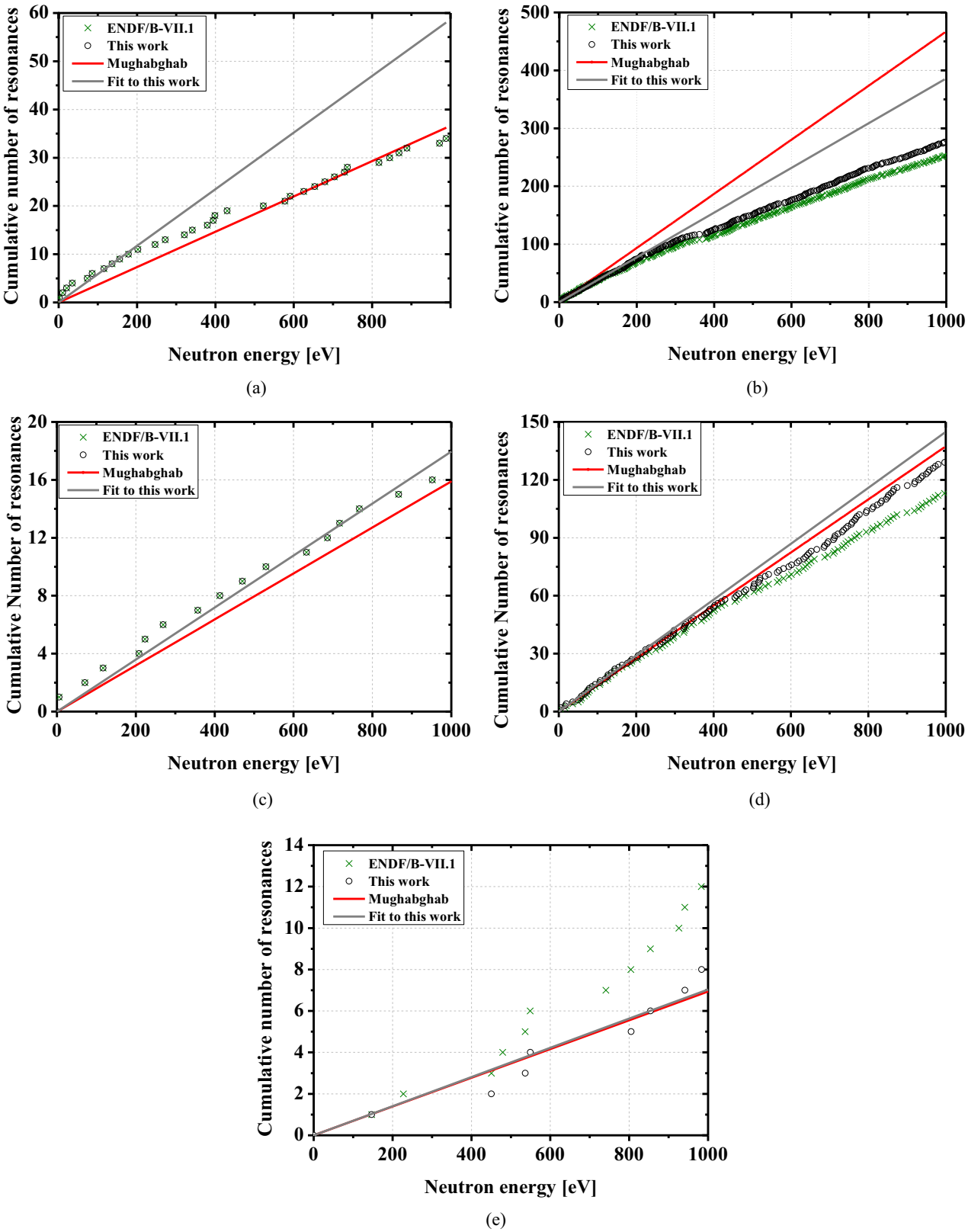

Fig. 4. Staircase plots of level densities for (a) ^{160}Dy, (b) ^{161}Dy, (c) ^{162}Dy, (d) ^{163}Dy, and (e) ^{164}Dy.

Table 11. The level densities of the dysprosium isotopes. The uncertainties in D_0 for this work are the uncertainties in the fitted slopes from fig. 4. The uncertainties in D_0 given in table 11 for the Atlas values are from Mughabghab [27].

Isotope	D_0 of this work [eV]	D_0 of Atlas [eV]
^{160}Dy	17.0 ± 0.8	27.3 ± 1.7
^{161}Dy	2.59 ± 0.01	2.14 ± 0.15
^{162}Dy	56 ± 1	62.9 ± 3.6
^{163}Dy	6.90 ± 0.08	7.28 ± 0.37
^{164}Dy	142 ± 7	144.1 ± 9.6

Table 12. Degrees of Freedom (DFs) of χ^2 distributions which were best matched with the reduced neutron width distributions.

Isotope	DF of this work	DF of ENDF
^{160}Dy	0.99	1
^{161}Dy	1.77	1.78
^{162}Dy	1.30	1.35
^{163}Dy	1.40	1.46

Statistical distributions of reduced neutron widths, Γ_n^0, were compared with ENDF/B-VII.1 for four isotopes in the region from 0 to 1000 eV. The statistical distribution for ^{164}Dy was not investigated because of the small number of resonances. Reduced neutron widths were divided by the average reduced neutron width, $\langle \Gamma_n^0 \rangle$, and cumulative distributions of these ratios were compared with the integral of the Porter-Thomas distribution [28] (χ^2 distribution with one degree of freedom). The degrees of freedom, DF, of a χ^2 distribution which are best matches with the data for each isotope are listed in table 12 and the distributions are plotted in fig. 5. The results agree reasonably with the Porter Thomas distributions. However, there are more narrow resonances than expected for ^{161}Dy and ^{163}Dy. These trends agree with the distribution of ENDF/B-VII.1 resonance parameters.

Statistical distributions of radiation widths were compared with those of ENDF/B-VII.1 for ^{161}Dy and ^{163}Dy in fig. 6. Only sensitive Γ_γ's, determined by the criteria in sect. 4.2, were used in the analysis. Radiation widths were divided by the error-weighted average radiation width, $\langle \Gamma_\gamma \rangle$. These values were fitted with χ^2 distribution varying degrees of freedom. χ^2 distributions with 584 and 110 degrees of freedom were best matched with radiation width distribution of ^{161}Dy and ^{163}Dy, respectively. The data are in reasonable agreement with the theory for multiple exit channels.

Neutron strength functions, S_0, were calculated for ^{161}Dy and ^{163} Dy. The values and those of ENDF/B-VII.1 [22] and the Atlas of Neutron Resonances [27] are listed in table 13. The S_0 values were determined from the resonances within the energy range where the level density is constant. The uncertainties given in table 13 were determined by a quadrature sum of the uncertainties in tables 5–9. S_0 for both ^{161}Dy and ^{163}Dy are larger than those from ENDF/B-VII.1. Otherwise, the values are smaller than those from the Atlas.

6 Conclusions

The multilevel R-matrix Bayesian code SAMMY was used to extract the resonance parameters from capture data sets for dysprosium isotopes and from a transmission data set of natural dysprosium. Resolution broadening, Doppler broadening, and multiple scattering correction of capture data were included during the fitting.

We observed 29 and 17 new resonances not listed in ENDF/B-VII.1 from ^{161}Dy and ^{163}Dy isotopes, respectively. Six resonances from ^{161}Dy isotope, two resonances from ^{163}Dy, and four resonances from ^{164}Dy listed in ENDF/B-VII.1 were not observed in the present measurements.

The capture resonance integrals of each isotope in the energy range from 0.5 eV to 20 MeV were calculated using the resulting resonance parameters. The capture resonance integrals were compared to the resonance integrals calculated with the ENDF/B-VII.1 parameters. The resonance integral value of the natural dysprosium calculated with present resonance parameters was 1405 ± 3.5 barn. The value is $\sim 0.3\%$ higher than that obtained with the ENDF/B-VII.1 parameters.

The average level spacing was measured. The D_0 for ^{160}Dy, ^{161}Dy, ^{162}Dy, ^{163}Dy, and ^{164}Dy were 17.04 ± 0.81, 2.59 ± 0.01, 55.69 ± 0.99, 6.90 ± 0.08, and 142.15 ± 6.87 eV, respectively.

The distributions of reduced neutron widths for ^{160}Dy, ^{161}Dy, ^{162}Dy, and ^{163}Dy were compared to those of ENDF/B-VII.1 and the theoretical Porter-Thomas distribution. The results agree reasonably with the Porter Thomas distributions. However, there are more narrow resonances than expected for ^{161}Dy and ^{163}Dy. For ^{161}Dy and ^{163}Dy, there are more narrow resonances than expected.

Statistical distributions of radiation widths were investigated for ^{161}Dy and ^{163}Dy and compared to ENDF/B-VII.1 and χ^2 distributions. The best-fits of ^{161}Dy and ^{163}Dy were χ^2 distributions with 584 and 110 degrees of freedom, respectively, which is in reasonable agreement with the theory for multiple exit channels.

Neutron strength functions were calculated for ^{161}Dy and ^{163}Dy. S_0 for both ^{161}Dy and ^{163}Dy are larger than those from ENDF/B-VII.1. Otherwise, the values are smaller than those from Atlas.

This research was partly supported by the Institutional Activity Program of KAERI, 2017 and by the National R&D Program through the Dong-nam Institute of Radiological & Medical Sciences (50491-2017).

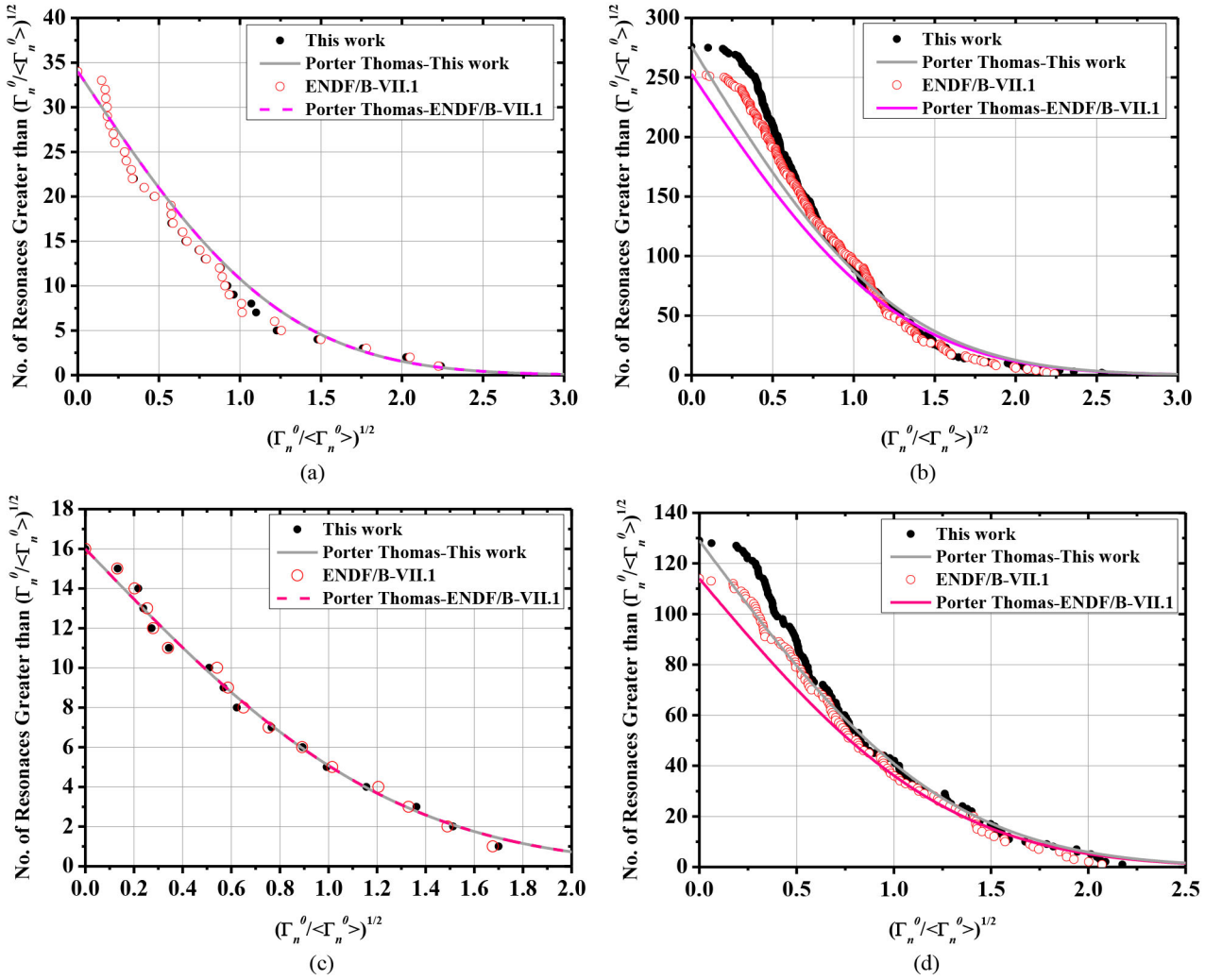

Fig. 5. Cumulative reduced neutron width distributions for the present measurements and ENDF/B-VII.1 of (a) ^{160}Dy, (b) ^{161}Dy, (c) ^{162}Dy, and (d) ^{163}Dy. The new resonances were included in these plots.

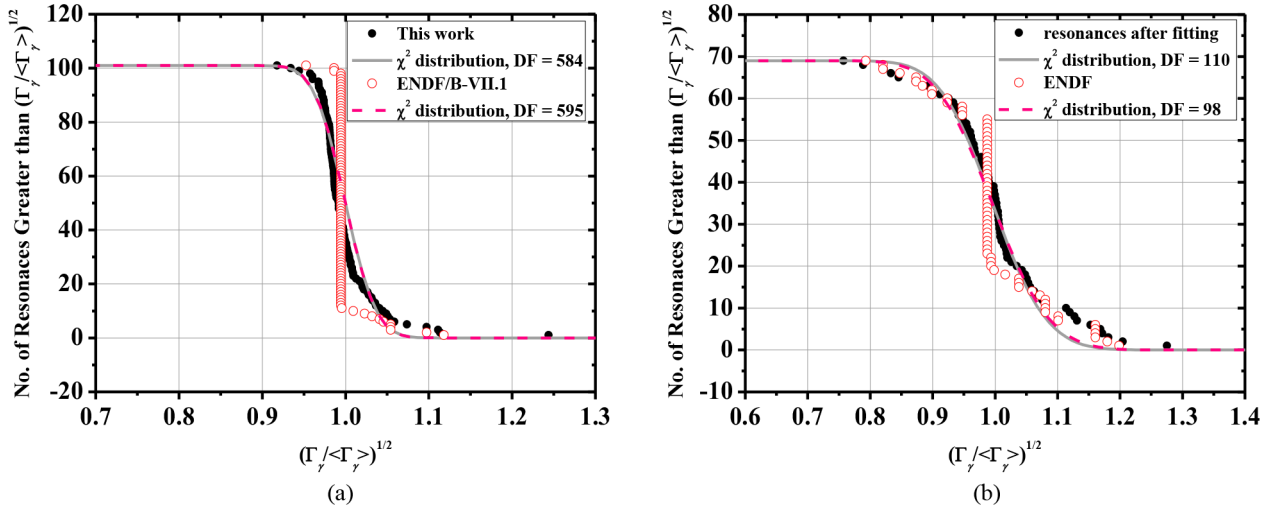

Fig. 6. Cumulative radiation width distributions for the present measurements and ENDF/B-VII.1 of (a) ^{161}Dy and (b) ^{163}Dy. Only the sensitive radiation widths were used for these plots.

Table 13. Neutron strength function, S_0, for ^{161}Dy and ^{163}Dy. The uncertainties given were determined by a quadrature sum of the uncertainties from tables 5–9.

	S_0 of ^{161}Dy $[10^{-4} \times \mathrm{eV}^{-1/2}]$	S_0 of ^{163}Dy $[10^{-4} \times \mathrm{eV}^{-1/2}]$
This work	1.66 ± 0.01	1.85 ± 0.02
ENDF/B-VII.1	1.58	1.61
Atlas of Neutron Resonances	1.82 ± 0.11	1.9 ± 0.2

References

1. D.R. Lide, *CRC Handbook of Chemistry and Physics*, 88th edition (CRC press, 2008).
2. R.C. Block *et al.*, Prog. Nucl. Energy **94**, 126 (2017).
3. N.M. Larson, ORNL/TM-9179/R8 and ENDF-364/R2 (2008) unpublished.
4. H.I. Liou, G. Hacken, J. Rainwater, U.N. Singh, J. Phys. Rev. C **11**, 462 (1975).
5. A.B. Popov, K. Tshetsyak, H.C. Gou, Sov. J. Nucl. Phys. **32**, 310 (1980).
6. H. Beer, R.L. Macklin, G. Walter, P.J. Pachet, J. Phys. Rev. C **30**, 464 (1984).
7. G. Kim, R. Machrafi, H. Ahmed, D. Son, V. Skoy, Y.S. Lee, M.-H. Cho, H. Kang, I.S. Ko, W. Namkung, J.H. Chang, K.J. Yoo, Ann. Nucl. Energy **30**, 1123 (2003).
8. R.L. Zimmerman, Bull. Am. Phys. Soc. **2**, 42(NA9) (1957).
9. G. Brunhart, H. Marshak, C.A. Reynolds, V.L. Sailor, R.I. Schermer, F.J. Shore, Bull. Am. Phys. Soc. **7**, 305(k16) (1962).
10. G. Brunhart, H. Postma, D.C. Rorer, V.L. Sailor, L. Vanneste, Z. Naturforsch. A **26**, 334 (1971).
11. S.F. Mughabghab, R.E. Chrien, Phys. Rev. C **1**, 1850 (1970).
12. E.N. Karzhavina, K.-S. Su, A.B. Popov, EXFOR/CINDA Database; `www.nndc.bnl.gov`, NNDC CINDA EXFOR Accession #40405 (1973).
13. E.N. Karzhavina, K.-S. Su, A.B. Popov, K. Faykov, EXFOR/CINDA Database; `www.nndc.bnl.gov`, NNDC CINDA EXFOR Accession #40410 (1986).
14. J. Brunner, F. Widder, EXFOR/CINDA Database; `www.nndc.bnl.gov`, NNDC CINDA EXFOR Accession #21025 (1967).
15. G.G. Slaughter, O.A. Wasson, S.F. Mughabghab, R.E. Chrien, EXFOR/CINDA Database; `www.nndc.bnl.gov`, NNDC CINDA EXFOR Accession #10822 (1972).
16. R. Sher, S. Tassan, E.V. Weinstock, A. Hellsten, EXFOR/CINDA Database; `www.nndc.bnl.gov`, NNDC CINDA EXFOR Accession #12098 (1961).
17. Y.-R. Kang *et al.*, Nucl. Sci. Eng. **180**, 86 (2015).
18. M.E. Overberg, B.E. Moretti, R.E. Slovacek, R.C. Block, Nucl. Instrum. Methods Phys. Res. A **438**, 253 (1999).
19. E.M. Baum, M.C. Ernesti, H.D. Knox, T.R. Miller, A.M. Watson, *Chart of the Nuclides*, 17th edition (Knolls Atomic Power Laboratory, Schenectady, 2010).
20. Rian M. Bahran, PhD Thesis, Rensselaer Polytechnic Institute (2013).
21. D.P. Barry, PhD Thesis, Rensselaer Polytechnic Institute (2003).
22. M.B. Chadwick *et al.*, Nucl. Data Sheets **112**, 2887 (2011).
23. E. Padovani, S.A. Pozzi, MCNP-POLIMI User's Manual (Library of Nuclear Engineering Dept., Polytechnic of Milan, Italy, 2002).
24. Y. Danon *et al.*, Nucl. Sci. Eng. **187**, 291 (2017).
25. R.E. MacFarlane *et al.*, LA-UR-12-27079 (2012) unpublished.
26. C.L. Dunford, USCD1212/07 (2005) unpublished.
27. S.F. Mughabghab, *Atlas of Neutron Resonances*, 5th edition (Elsevier, New York, 2006).
28. C.E. Porter, R.G. Thomas, Phys. Rev. **104**, 483 (1956).